The Abdus Salam
International Centre
for Theoretical Physics
50th Anniversary 1964–2014

2585-19

Joint ICTP-TWAS School on Coherent State Transforms, Time-Frequency and Time-Scale Analysis, Applications

2 - 20 June 2014

Cellular mechanics is a multi scaling phenomena: a few examples

F. Argoul
ENS, Lyon, France

Cellular mechanics is a multi scaling phenomena: a few examples

F. Argoul, L. Berguiga, C. Martinez, E. Provera, A. Arneodo, J. Elezgaray[*], B. Laperrousaz, V. Maguer-Satta*[**], T. Voeltzel*[**]

UMR5672 CNRS, Physics Laboratory - ENS Lyon
[*] UMR5248 CNRS-Université Bordeaux 1, Pessac
[**] CRCL, Research Center for Cancer of Lyon, CLB Lyon.

The cellular metabolism

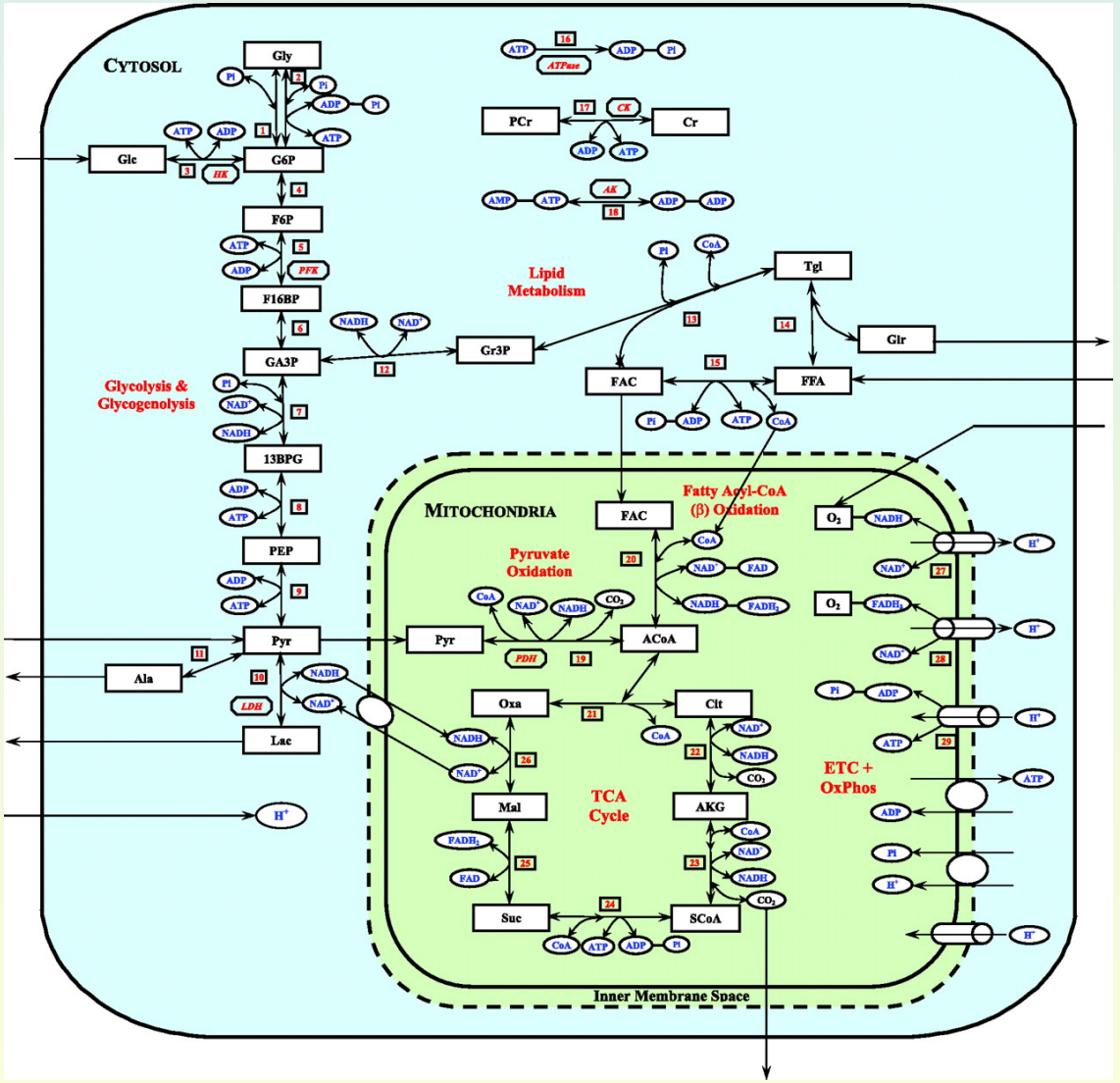

The metabolism is made by the biochemical engines of the cells. Knowing each of the metabolic cycle does not gives the answer on how the cell behaves in different environments.

CELL DYNAMICS is MULTISCALED in TIME and in SPACE

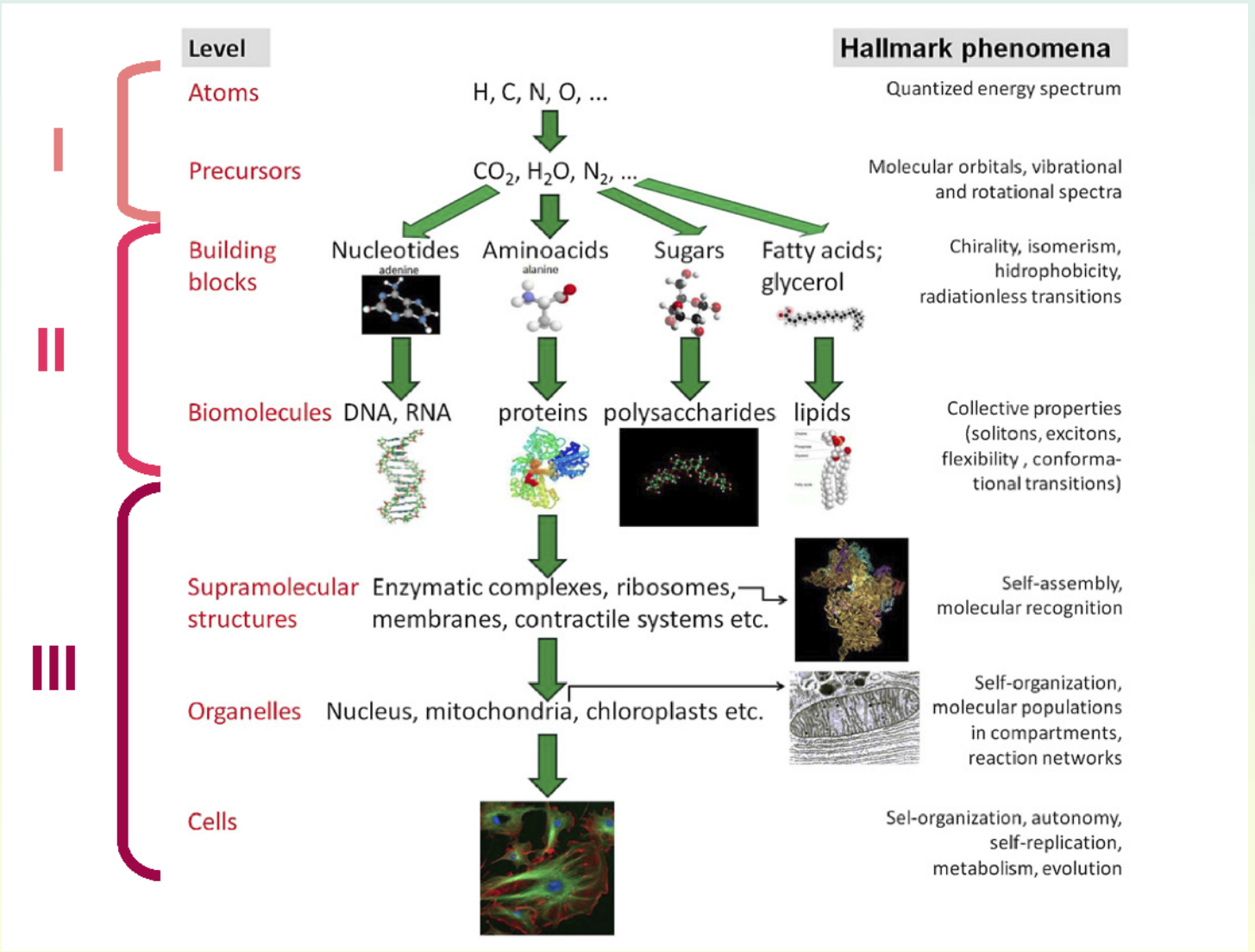

From the atoms to the cells, at least three integration steps can be outlined

CELL DYNAMICS is MULTISCALED in TIME and in SPACE

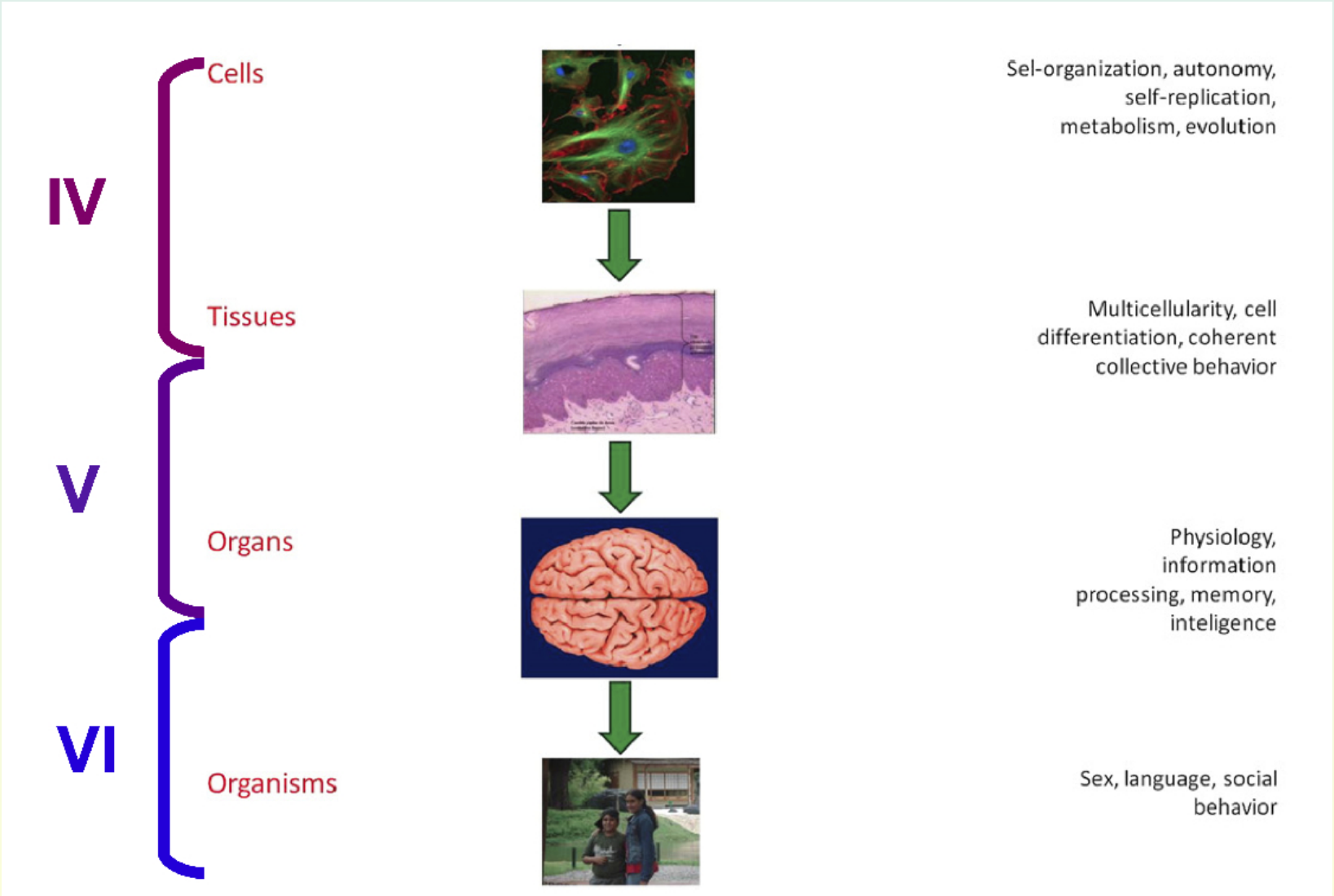

From cells to organisms, we can delineate three integration steps

Tumour growth is a multi-scale process

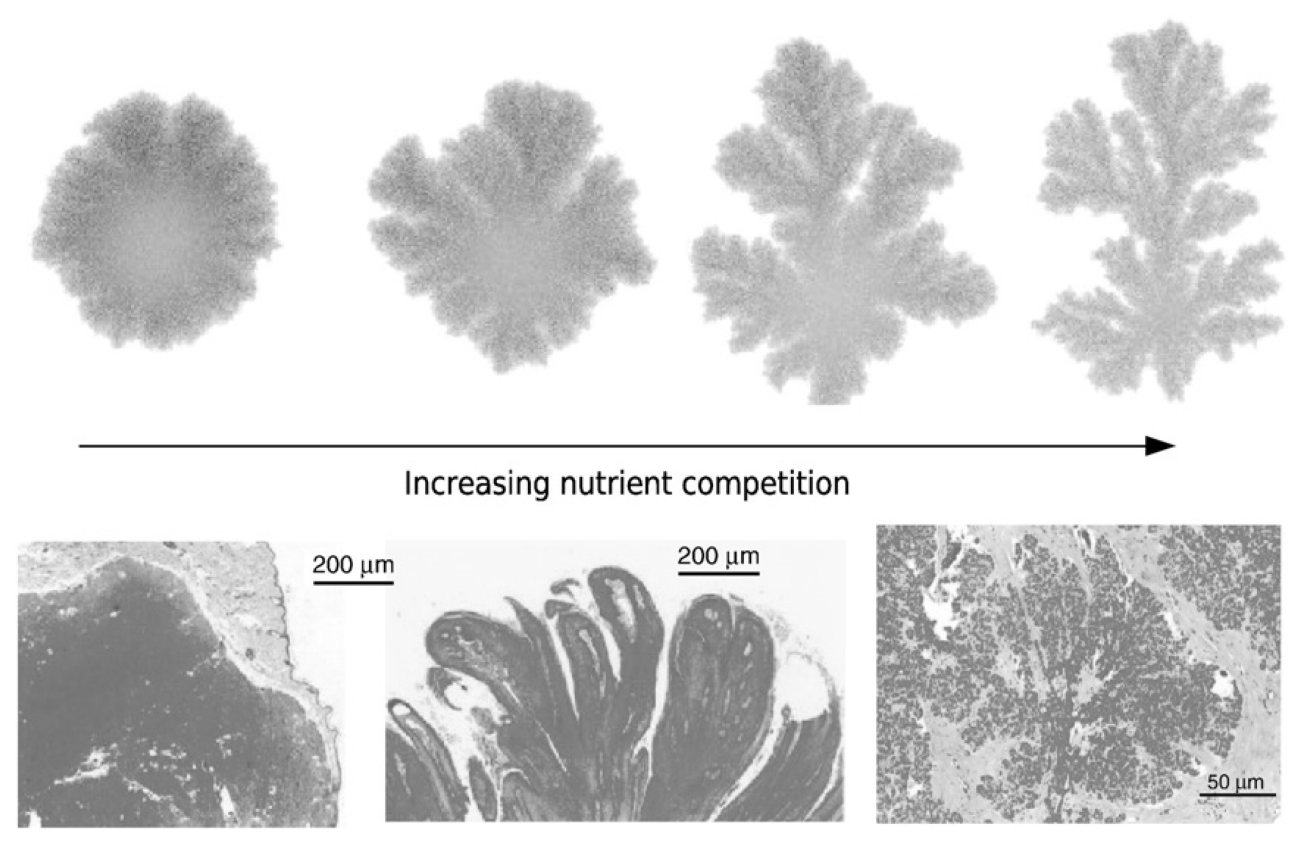

Top: Simulated patterns generated by the nutrient-limited cancer growth model
Bottom: common morphologies observed in cancer. From left to right, a compact solid basocellular carcinoma, a papillary pattern of a squamous papyloma, and the characteristic ramified morphology of trichoblastomas. *[M. Ferreira Vilela Cur. Op. Col. Interf. Science 2010]*

Physical approaches of biological systems: a question of spatial and temporal scales

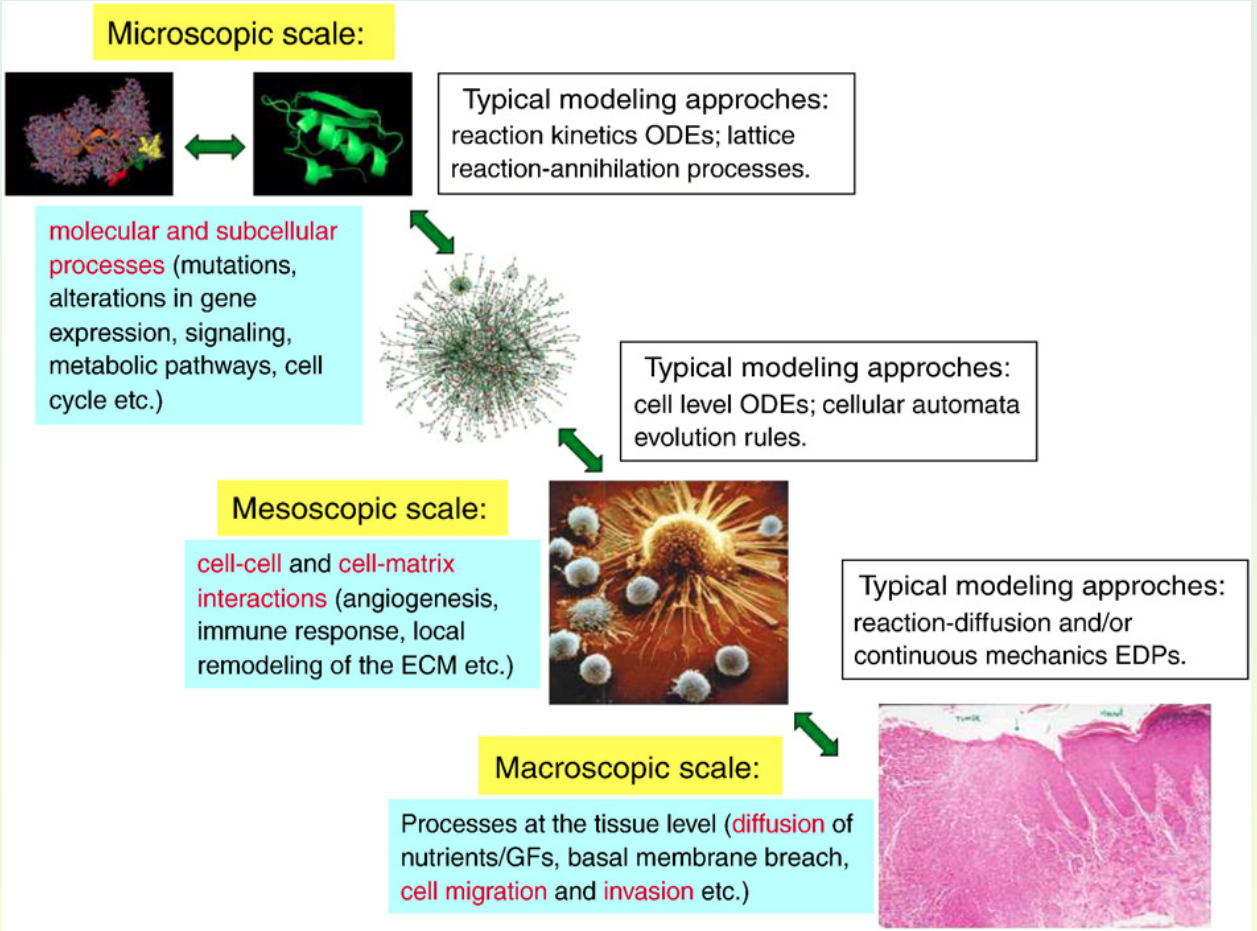

Hierarchy of scales and the related mechanisms and modeling approaches. The arrows indicate the mutual interdependence between the levels in multiscale modeling of cancer growth, implying that models/subsystems at a given scale use information from another scales.
[M. Ferreira Villela Cur. Op. Col. Interf. 2010]

From 2D to 3D environment: cells sense the space around them

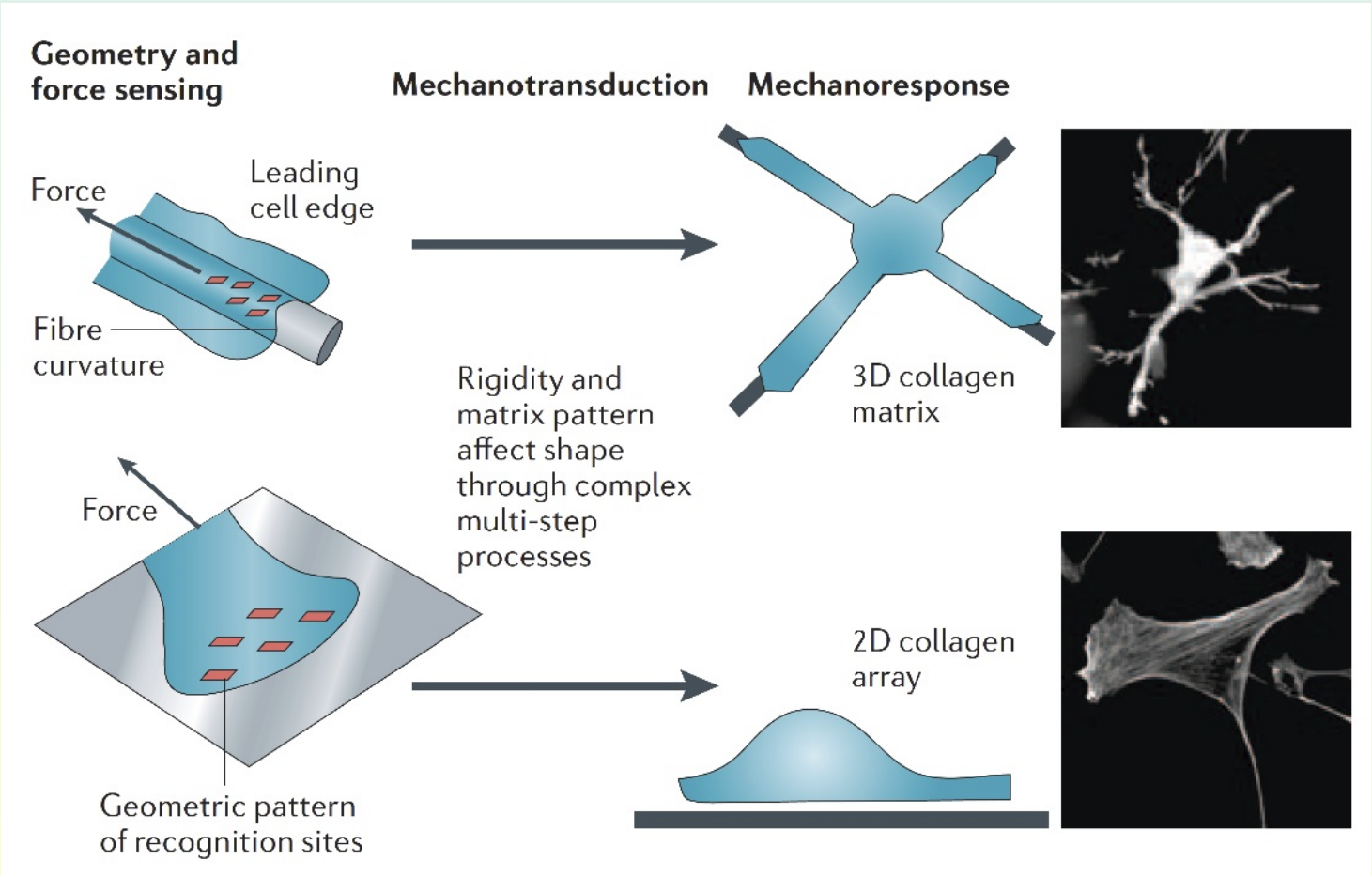

Human fibroblasts project a dendritic network of extensions in collagen matrices [top] but not on collagen-coated coverslips [bottom] (4 hours incubation) *[Grinnel, Mol. Biol. of the Cell, 2003]*

Cells are stretching and tensing systems

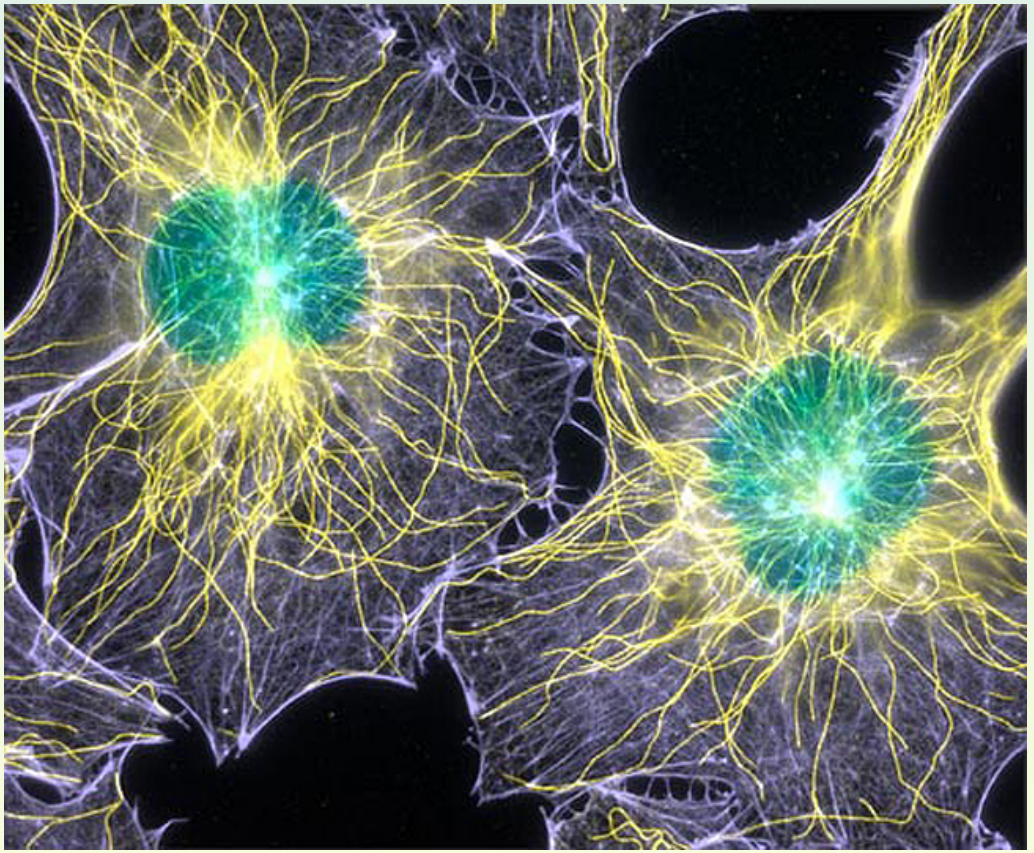

The microtubules are stained in yellow,
there is an organisation of these filaments to preserve and maintain the cell shape.

Cells are stretching and tensing systems

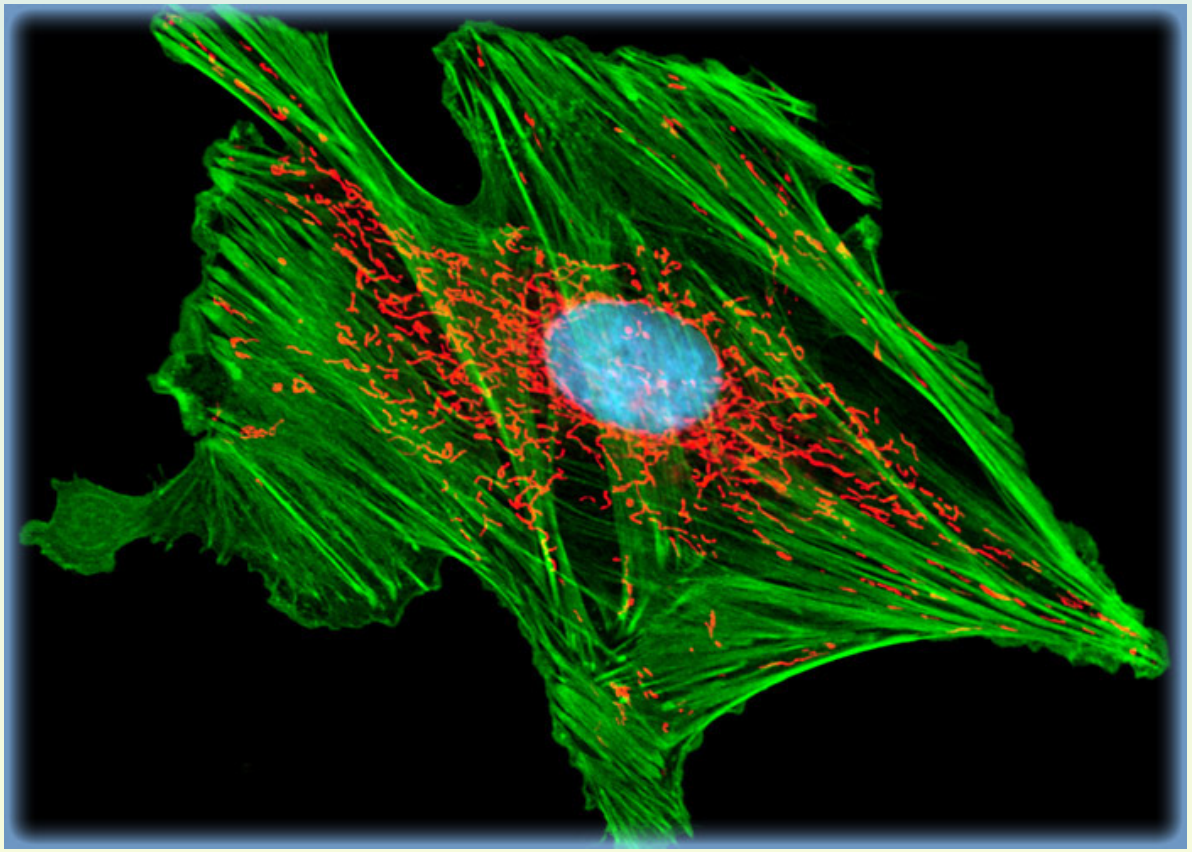

The actin stress fibers are staining in green,
these filaments elongate and grow to allow the cell contracting and stretching on adhesive support.
Actin and myosin are two proteins which contribute to cell locomotion. (in red the mitochondrial network, in blue the nucleus)

Cells are active systems that remodel in real time their shape

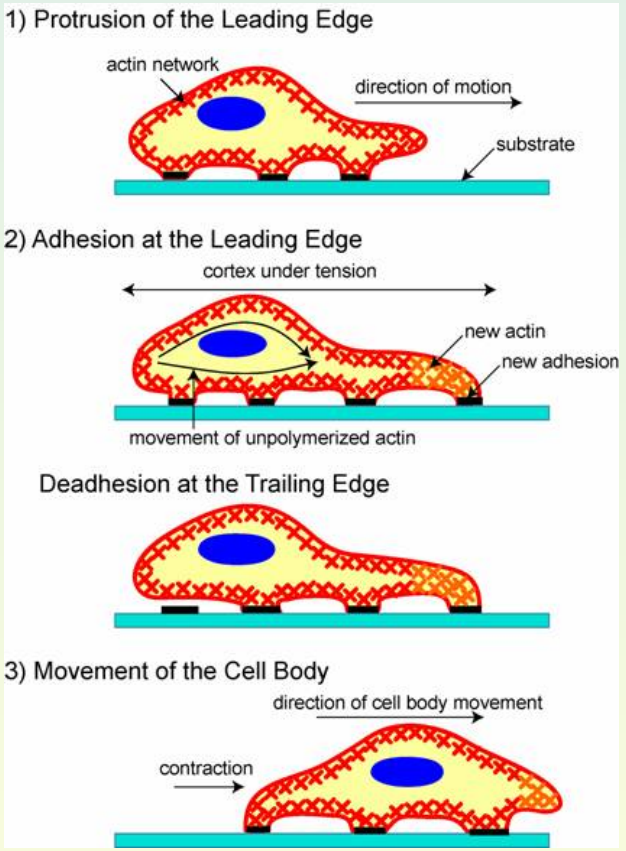

A cartoon to describe a cell motion (adherent cell))

A cartoon of mechanosensing

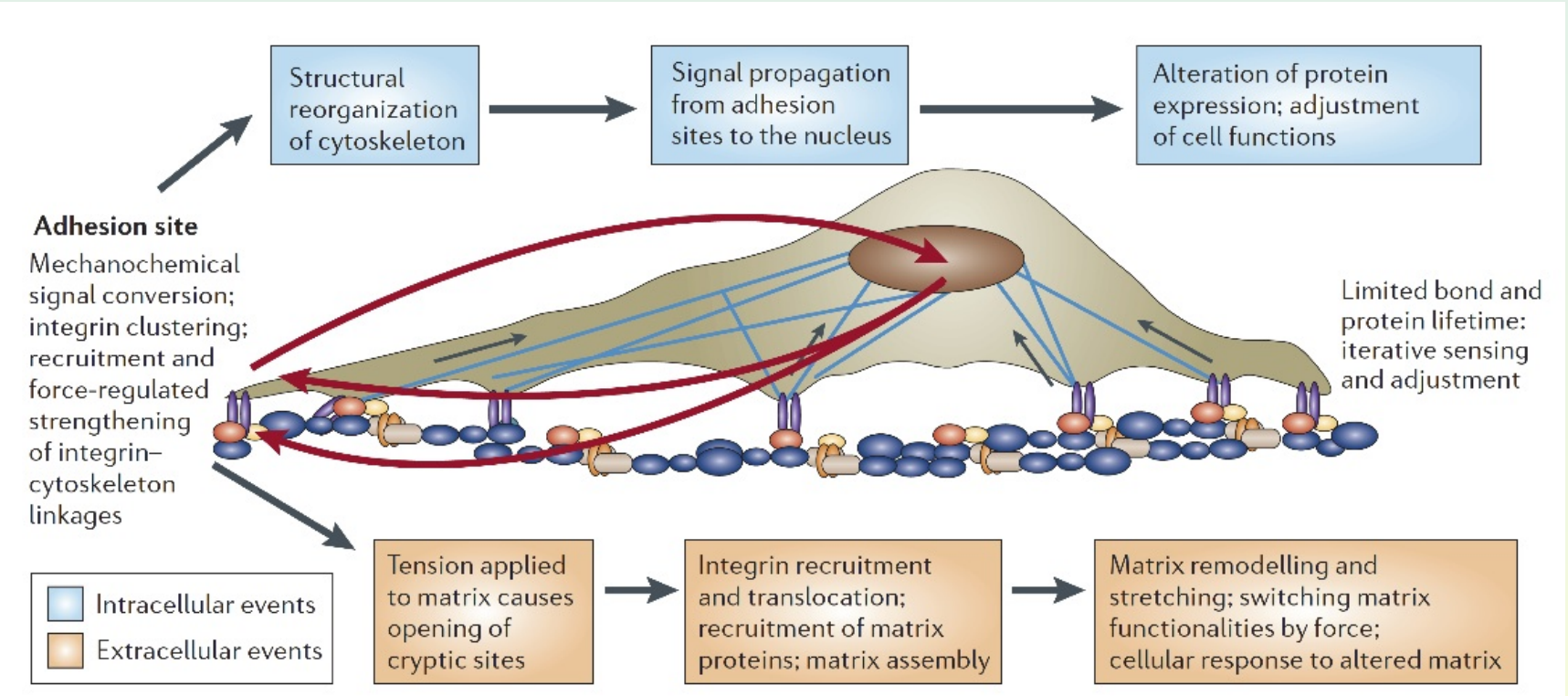

When cells sense the mechanical features of their environment, they pulls on their environment and produce a cascade of events inside and outside of their body. Outside, they modify the extracellular matrix and create new signals, such as those originating from fibronectin unfolding. Inside, intracellular signals alter the expression pattern of the cell and, over time, change the cell shape and its mechanical response *[Vogel, Nat. Rev. Mol. Cell Biol, 2006]*

Mechanically coupling the extracellular matrix with the nucleus

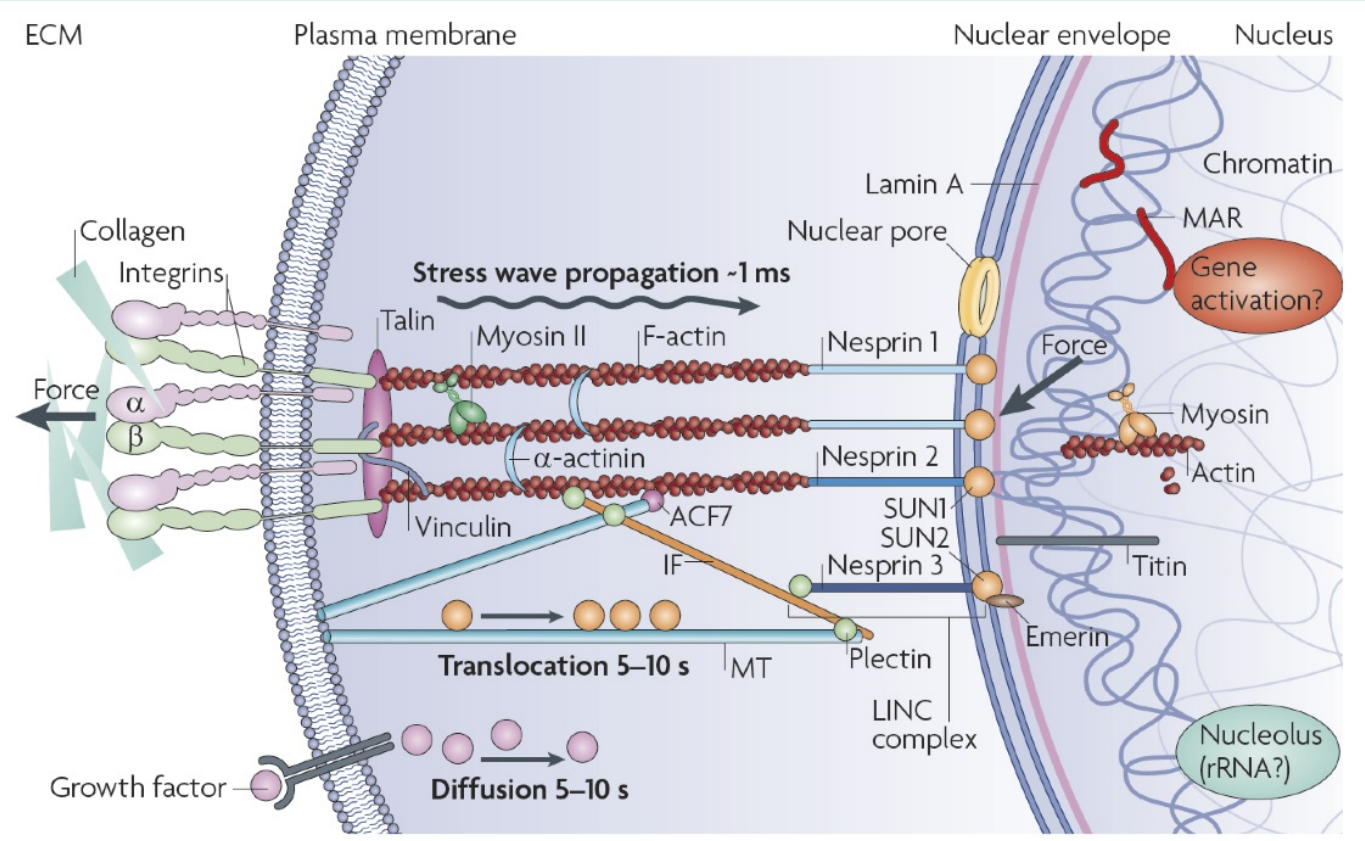

Forces channelled into the nuclear scaffold might directly affect gene activation within milliseconds of surface deformation. By contrast, it takes seconds for growth factors to alter nuclear functions by eliciting chemical cascades of signalling, which are mediated by motor-based translocation or chemical diffusion. LINC, linker of nucleoskeleton and cytoskeleton; rRNA, ribosomal RNA. *[Wang, Nat. Rev. Mol. Cell Biol. 2009]*

Models of cell rheology.

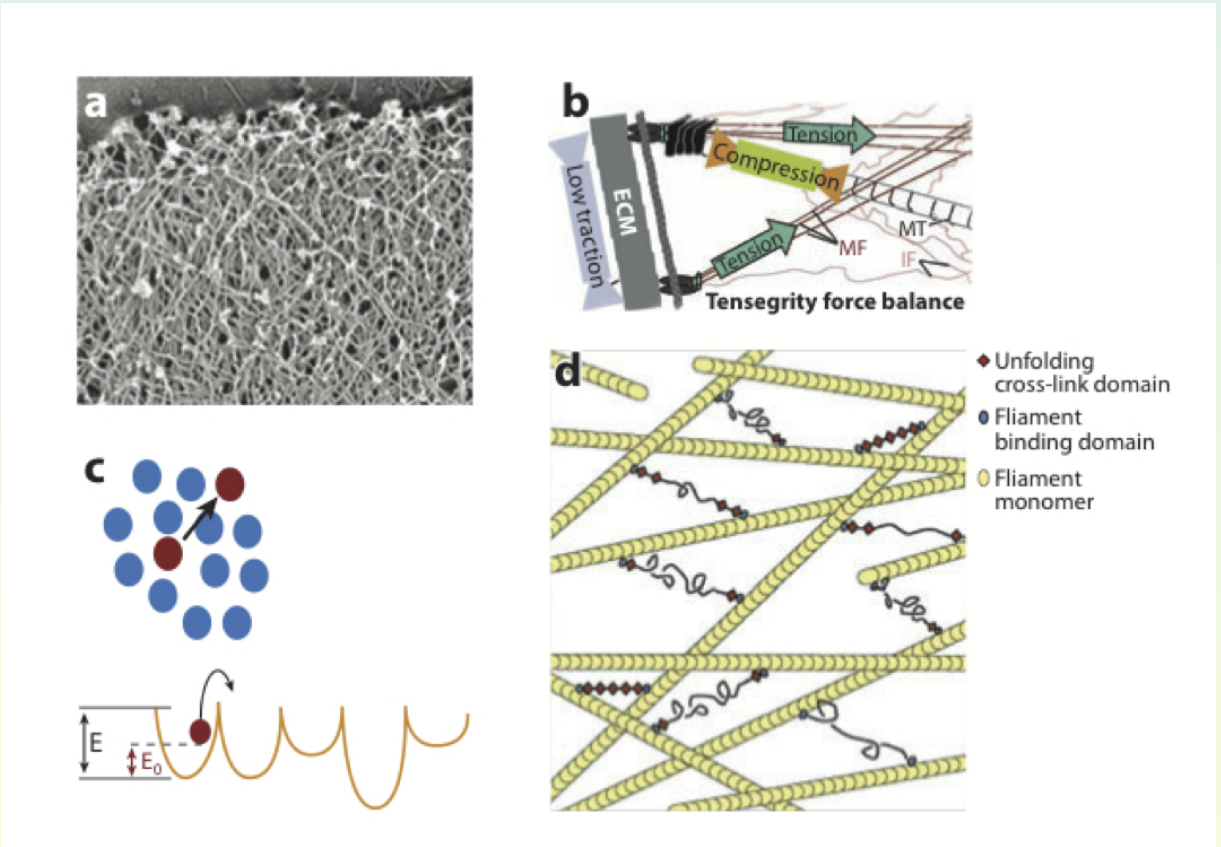

Cell rheology models proposed in the litterature: (a) EM of the lamellipodal actin network. (b) Schematic of the tensegrity model. (c) Schematic of soft glass rheology. (d) Dynamic cross-link models. *[B.D. Hofman, Annu. Rev. Biomed. Eng. 11 (2009) 259-88]*

Global quantities collected in cell mechanics

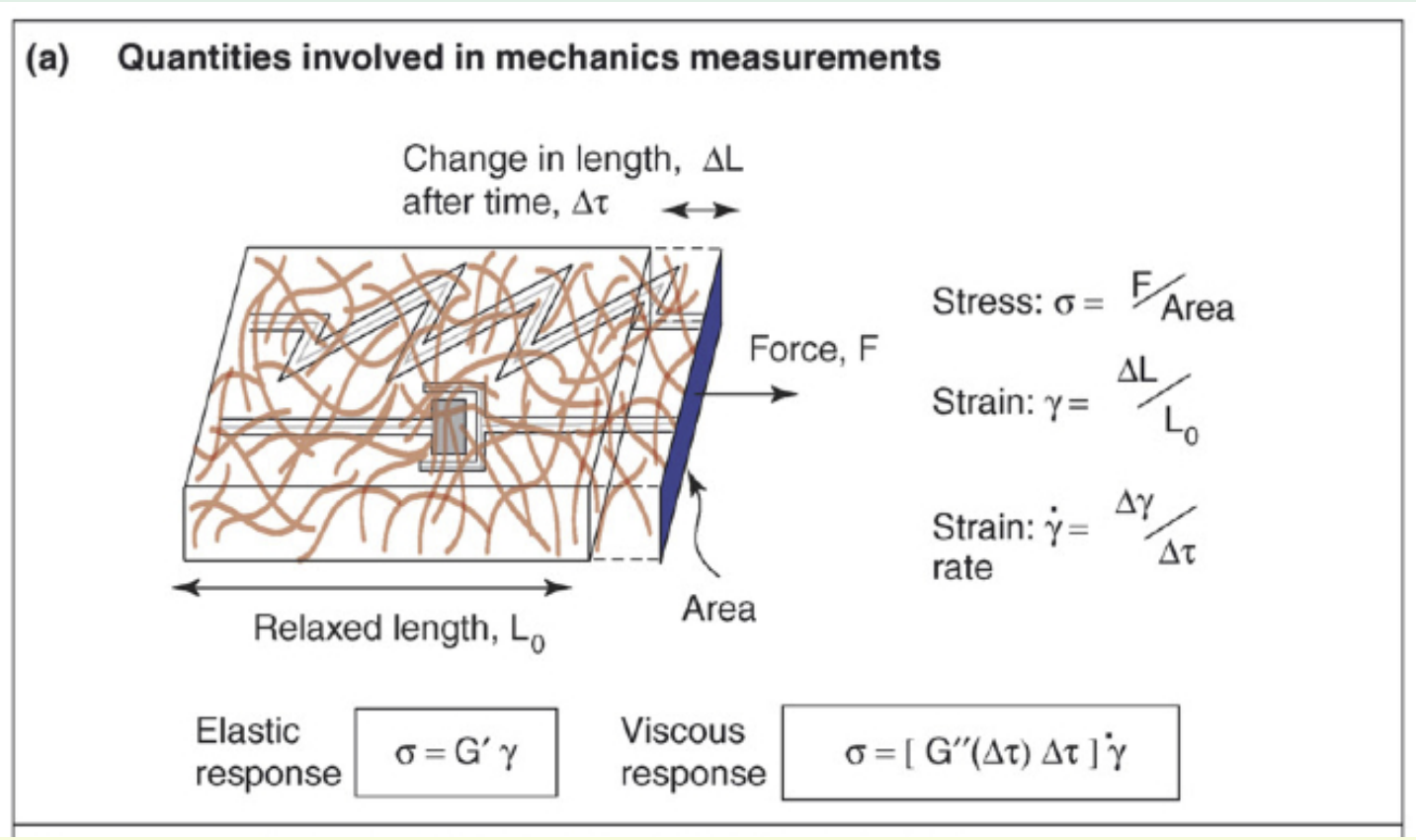

The shear modulus and its frequency dependence: a cartoon. *[Kasza Curr. Opinion Cell Biology 19 (2007) 101]*

Cell and touch: experimental methods of mechanical probes (1)

Bulk rheology
A material is sheared between two plates using an oscillatory stress to probe the shear elastic, G', (in-phase) and viscous, G'', (out-of-phase) moduli.

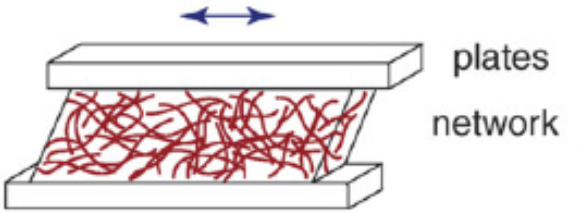

Magnetic bead cytometry
An external magnetic field applies a stress to a magnetic bead. The bead is position tracked to determine the response.

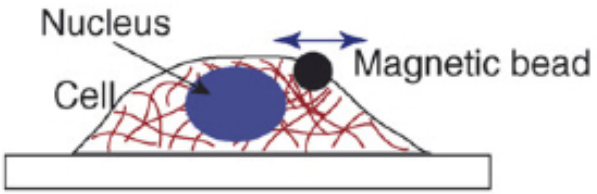

Traction force microscopy
Cell contractions deform a flexible substrate. Forces are estimated from bead displacements.

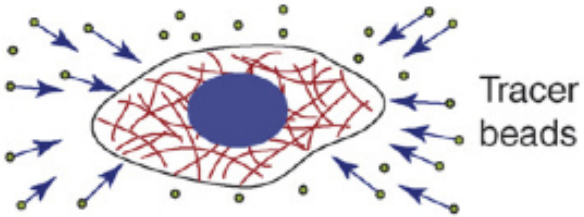

Experimental methods that have been designed to measure the rheological response of cells *[Kasza Curr. Opinion Cell Biology 19 (2007) 101]*

Cell and touch: experimental methods of mechanical probes (2)

Atomic force microscopy
A cantilever applies stress to the cell. The cantilever deflection is measured by laser reflection.

Microrheology
The motion of probe particles is measured using either video or laser tracking techniques. Particle motion is either driven externally or thermally induced and is interpreted to yield the viscoelastic modulus.

Whole cell stretching
A cell is attached to two surfaces. A force is applied to one surface and the plate separation is measured.

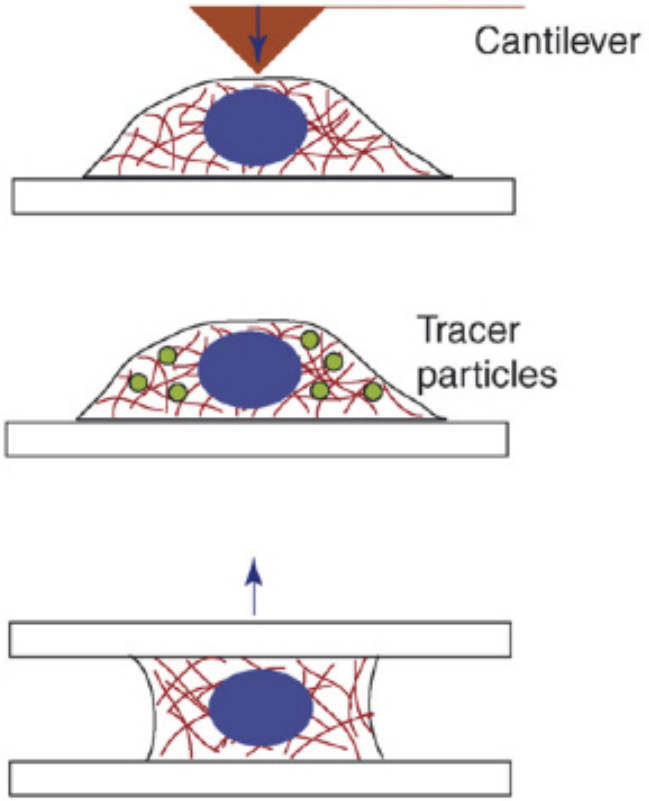

Experimental methods that have been designed to measure the rheological response of cells
[Kasza Curr. Opinion Cell Biology 19 (2007) 101]

Understanding linear versus nonlinear rheology and stress stiffening.

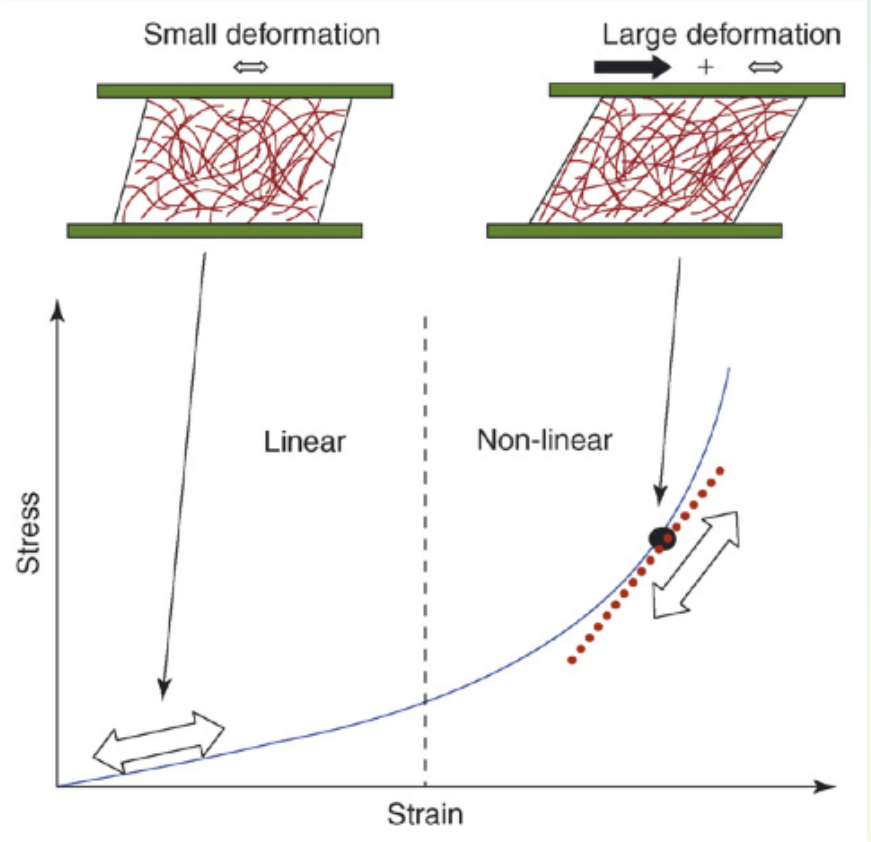

Under small deformations, the stress is proportional to the strain and the material is said to be in the linear regime. Under large deformations, the stress increases more rapidly with applied strain. Here the material is dais to be in the nonlinear regime. *[Kasza Curr. Opinion Cell Biology 19 (2007) 101]*

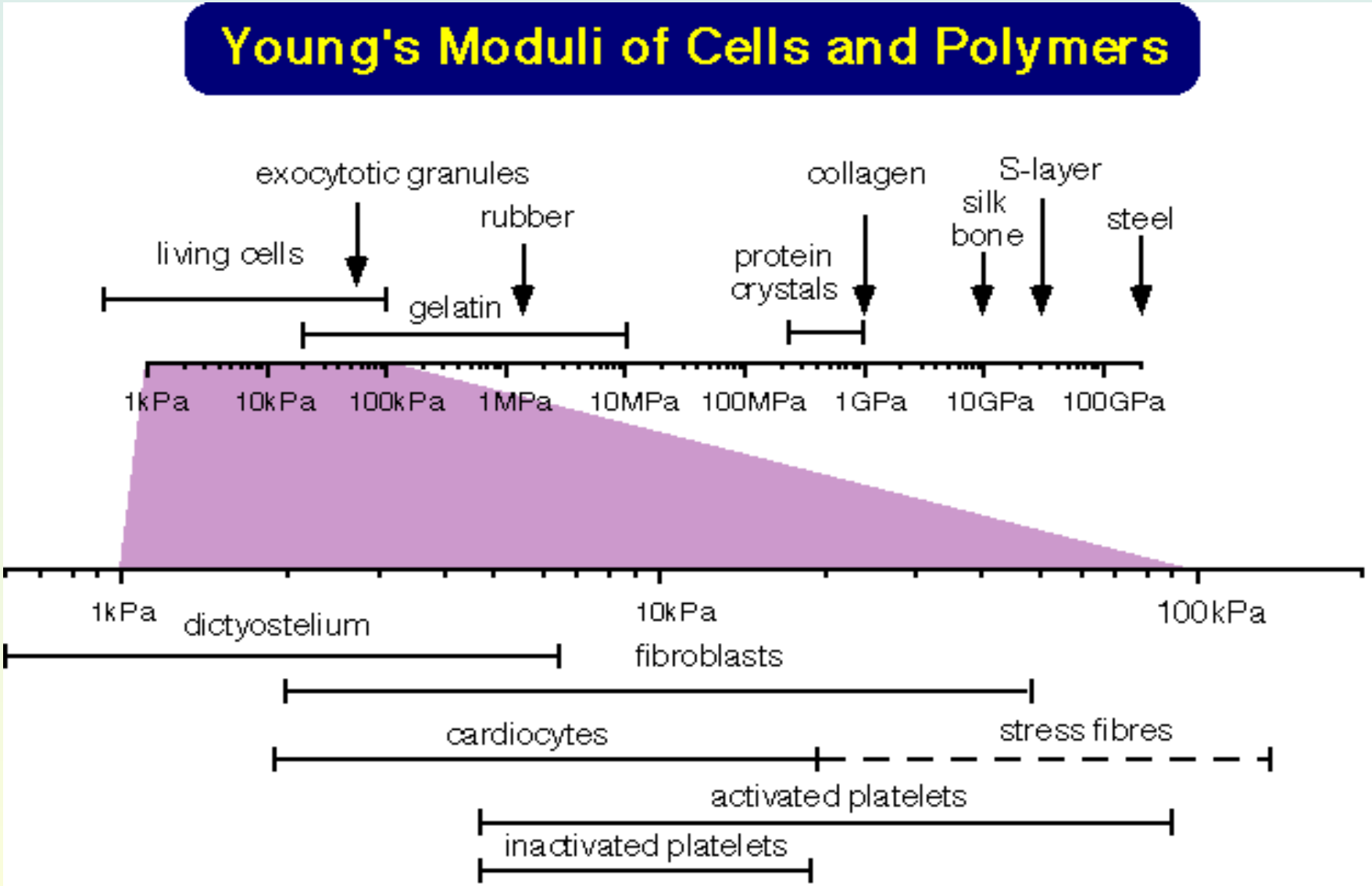

Manfred Radmacher
Universität München

Mechanical response of a single walled cell from Arabidopsis thaliana root call

The root tissue from which the single cells are extracted (3D reconstruction of a fluorescence image from confocal sections. The cellulose fibers are stained in white.

AFM: a mechanical sensor of cell viscoelasticity

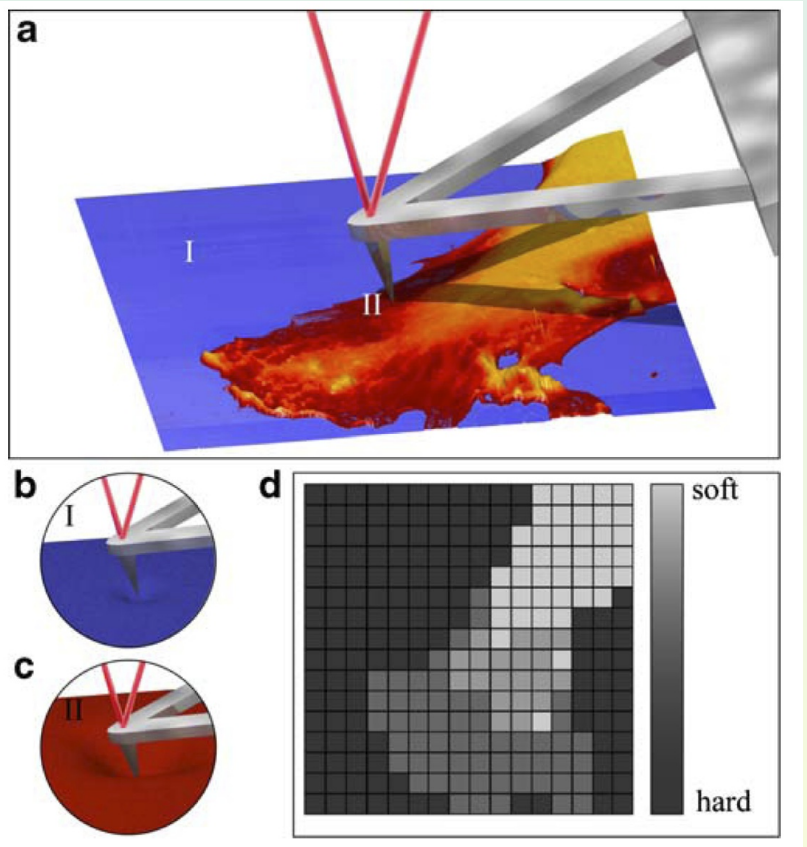

The AFM cantilever deflection is proportional to the force applied on its branches (V-shaped here). It can therefore differentiate a stiff (the glass for instance) and a soft (a cell) sample. Force maps (see d) can be reconstructed from force curves captured point by point. *[T. Ludwig, Pflugers Arch. Eur. J. Physiol. 2008]*

What forces does the AFM measure?

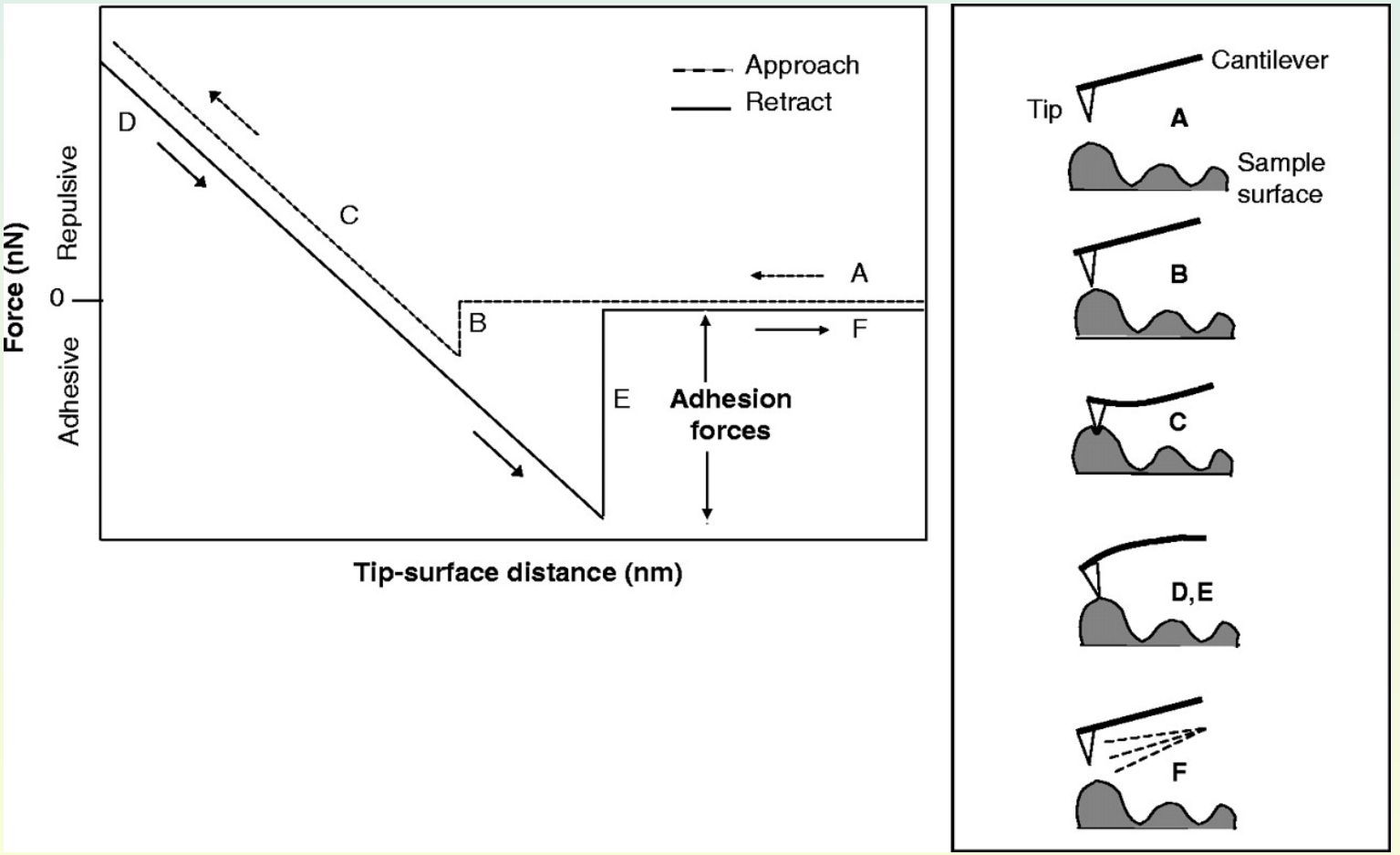

LOADING - UNLOADING FORCE CURVES

AFM force curves captured on one A. thaliana single cell

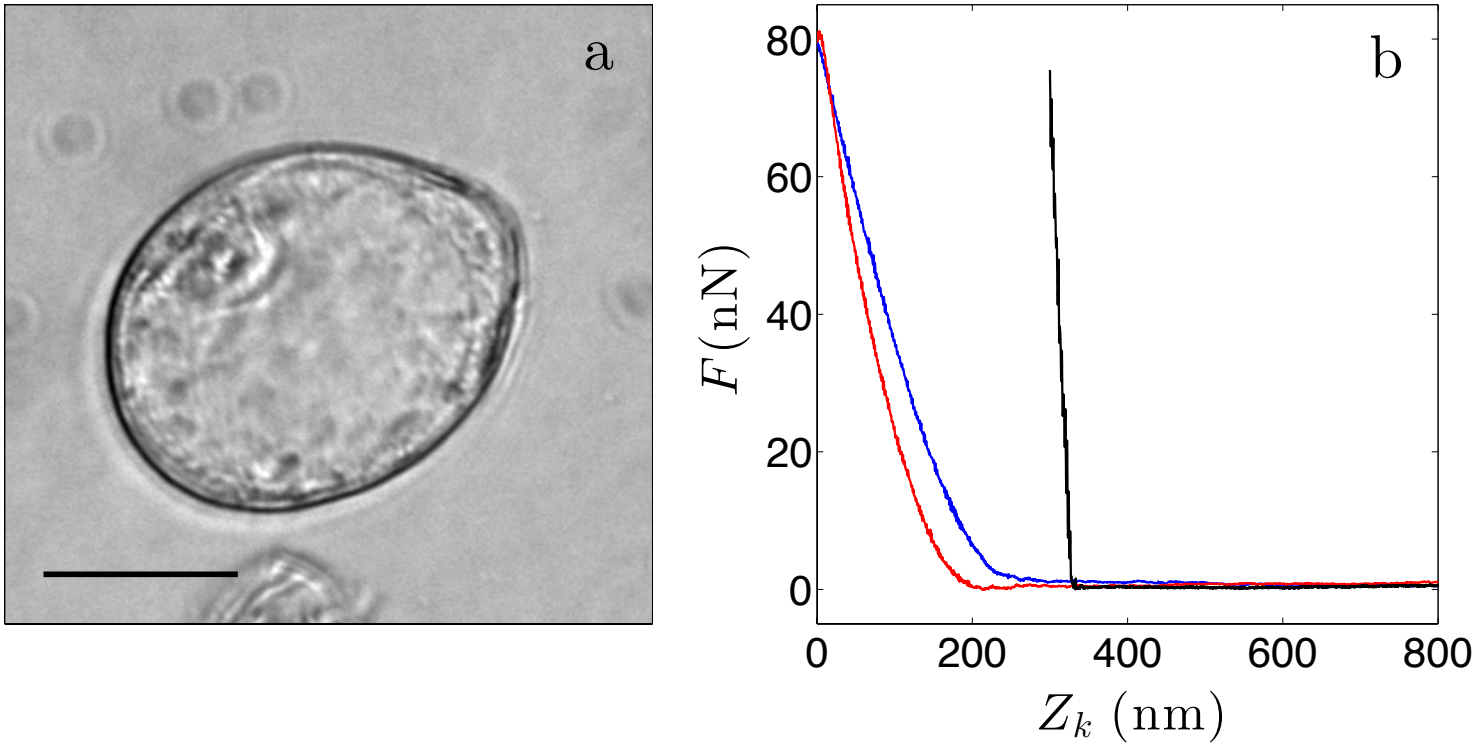

(a) Transmission microscopy of a single cell from *A. thaliana* root callus; the scale bar is 25 μm. (b) Untreated force curves recorded in liquid on the bottom of a petri dish (black line) and on a single cell, the blue (resp. red) line corresponds to the loading (resp. unloading) force curve.

Principle of AFM measurements

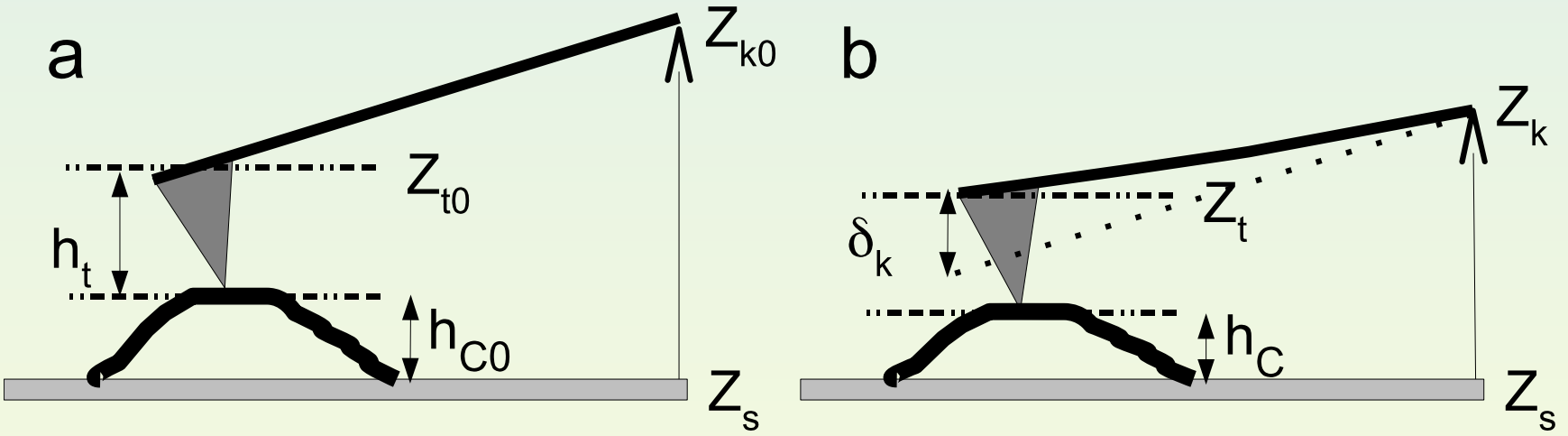

The principle of and AFM system: the deflection of the cantilever gives the force of interaction of the tip with the cell.

Deciphering the shapes of the approach force curves on A. thaliana single cells

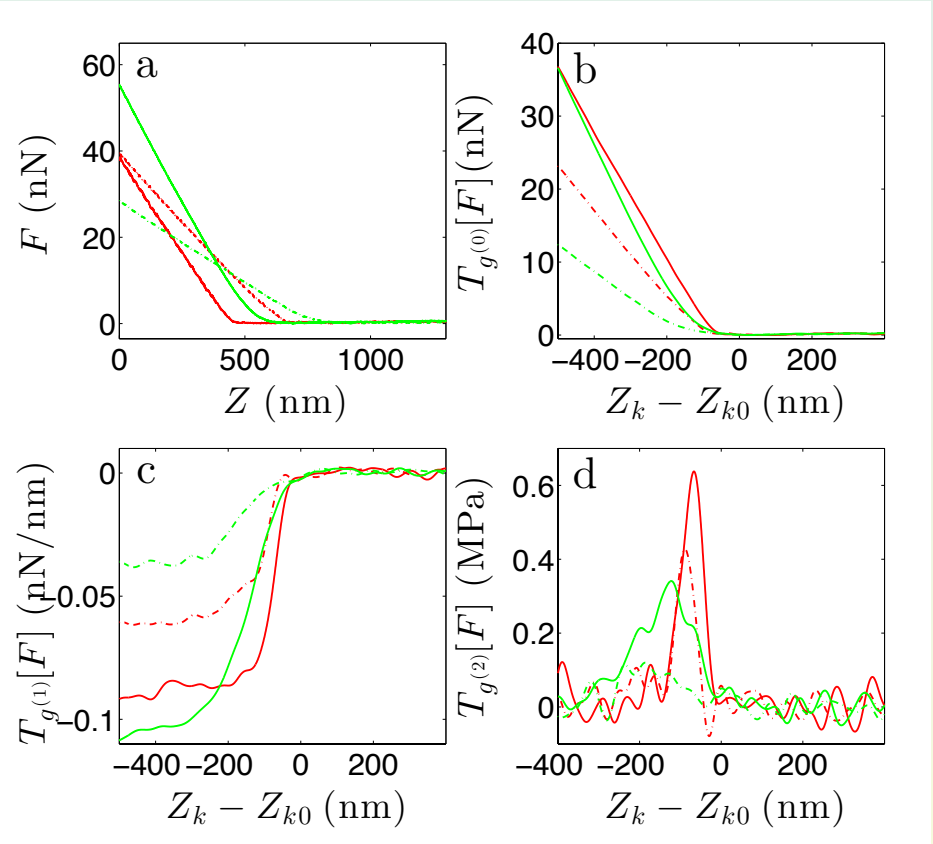

Experimental force curves collected on two different cells (approach). (a) Force-indentation curves. (b) Plot of $\mathcal{T}_{g(0)}[F]$ versus $Z_k - Z_{k0}$. Z_{k0} corresponds to $T_{contact} = -10^{-3}$ nN/nm. (c) Plot of $\mathcal{T}_{g(1)}[F]$ versus $Z_k - Z_{k0}$. (d) Plot of $\mathcal{T}_{g(2)}[F]$ versus $Z_k - Z_{k0}$.

A cartoon of the cell deformation

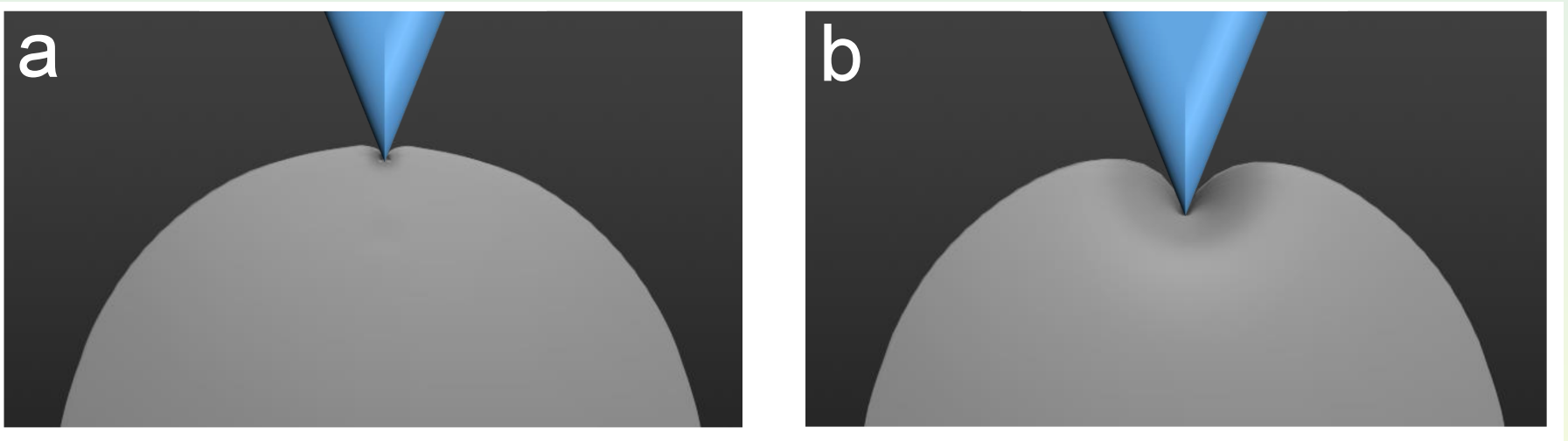

Sketch of the indentation of the cell wall by a pyramidal shape tip. (a) The tip penetrates the wall without changing noticeably its curvature (Regime A). (b) For a deeper indentation, the wall curvature is modified by the pyramidal tip (Regime B).

Physical model for describing the indentation of a walled cell (elastic shell) by a pyramidal shape indenter

For a given deflection of the cantilever (the contact force) the total displacement of the AFM piezo transducer is the sum of the cantilever deflection δ_k, the depth of penetration of the tip inside the wall δ_p and the deformation (change of curvature) of the wall δ_b.

$$\delta = Z_k - Z_{k0} = \delta_k + \delta_C = \delta_k + \delta_p + \delta_b \tag{1}$$

Correcting the force curves with the cantilever deflection δ_k, we get essentially the total indentation of the cell:

$$Z_k - Z_{k0} = \delta_C = \delta_p + \delta_b \ . \tag{2}$$

These two terms describe the shallow penetration of the wall by the tip (regime A) and the deformation of the wall (regime B) by a global bending and stretching.

Physical model for describing the indentation of a walled cell (elastic shell) by a pyramidal shape indenter

Regime A : two power laws can be observed:

- If $\delta_p \lesssim r_t$:

$$F(\delta_p) = \left[\frac{4E\sqrt{r_t}}{3(1-\nu^2)}\right]\delta_p^{3/2} \tag{3}$$

- In the limit $\delta_t \gg r_t$, and assuming that $\delta_t < H_w$:

$$F(\delta_p) = \left[\frac{\tan(\theta)E}{\sqrt{2}(1-\nu^2)}\right]\delta_p^{2} \tag{4}$$

E is the Young modulus of the wall, ν is the Poisson ratio, θ is half the tip angle, r_t is the radius of the tip of the cantilever. These two formula predict that if the wall is soft enough for being penetrated by the cantilever tip, we should first observe a power-law $\delta^{3/2}$ followed by a power-law δ^2, assuming that the wall is thick enough ($H_w \gg r_t$).

Physical model for describing the indentation of a walled cell (elastic shell) by a pyramidal shape indenter

Regime B : bending and stretching the wall
Here we put a general form for $F(\delta_b)$ with a nonlinearity exponent h that will generalize these linear response models to strain-hardening ($h > 1$) or strain-softening ($h < 1$) systems:

$$F(\delta_b) = K_E \ \ \delta_b^h \ . \tag{5}$$

K_E can be considered as an effective tension of the wall.

A simplified mathematical model:

$$\begin{array}{lll} F(Z_k) & = K_E(Z_k - Z^*)^h & \text{for } \ Z_k < Z_1 : \text{Regime B} \\ F(Z_k) & = A(Z_k - Z_0)^{3/2} & \text{for } \ Z_1 < Z_k < Z_0 : \text{Regime A} \\ F(Z_k) & = 0 & \text{for } \ Z_k \geq Z_0 \ . \end{array} \tag{6}$$

The mathematical model mimic the experimental force curves

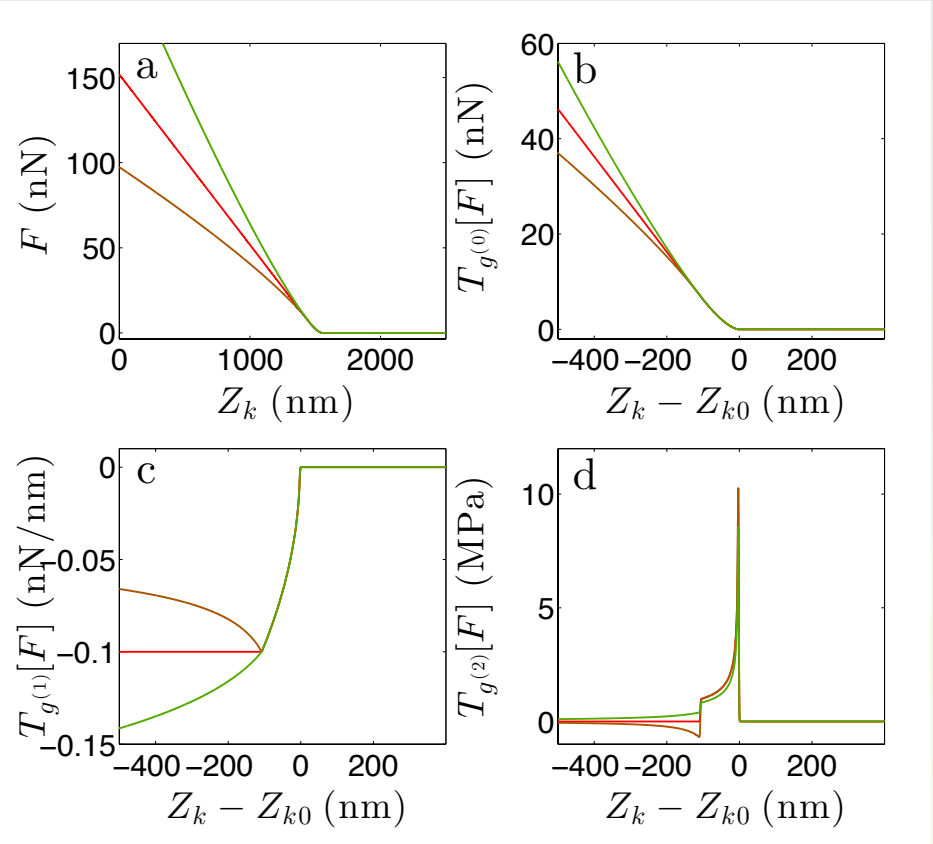

Computation of the first and second derivatives of the nonlinear force-curve model (Eq. 6) using the WT method with a Gaussian function ($sw_0 = 10$ nm). The green - red - brown curves correspond respectively to Hölder exponents $h = 1.2, 1$ and 0.8. ((a) The original force curves. (b) $\mathcal{T}_{g^{(0)}}[F](Z_k - Z_{k0}, s = 1)$, Z_{k0} corresponds to $T_{contact} = -10^{-4}$ nN/nm. (c) $\mathcal{T}_{g^{(1)}}[F](Z_k - Z_{k0}, s = 1)$ in nN/nm. (d) $\mathcal{T}_{g^{(2)}}[F](Z_k - Z_{k0}, s = 1)$ in MPa.

The multi-scale wavelet analysis to extract the holder exponent h

Within the norm $\mathcal{L}^1$, the one-dimensional WT of a signal $F(x)$ reads:

$$W_\psi[F](b,s) = \frac{1}{s}\int_{-\infty}^{\infty} F(x)\psi^*(\frac{x-b}{s})dx \ , \tag{7}$$

where b is a position and s (> 0) a scale parameter. A typical analyzing wavelet $\psi(x)$, that is admissible (of null integral) is the second derivative of a Gaussian $g^{(0)}(x) = e^{-x^2/2}$, also called the Mexican hat wavelet:

$$g^{(2)}(x) = -\frac{d^2}{dx^2}g^{(0)}(x) = e^{-x^2/2}(1-x^2) \ . \tag{8}$$

Via two integrations by part, we get the relation of the wavelet transform of F with the second derivative of a Gaussian wavelet $W_{g^{(2)}}[F](b,s)$ with the second derivative of F, smoothed by a Gaussian function $W_{g^{(0)}}[F](b,s)$:

$$W_{g^{(2)}}[F](b,s) = s^2\frac{d^2}{db^2}W_{g^{(0)}}[F](b,s) \ . \tag{9}$$

The multi-scale wavelet analysis to extract the holder exponent h

If the wavelet has a compact support, it has been demonstrated that the wavelet transform of F: $W_\psi[F](x_0, s)$ depends upon the values of $F(x)$ in a neighborhood of x_0 of size proportional to the scale s. If $F(x)$ behaves as $(x - x_0)^h$ in the neighborhood of x_0, then a straightforward calculation yields that the WT of F behaves as a power-law of the scale with the exponent h:

$$|W_\psi[F](x_0, s)| \propto A s^h \ . \tag{10}$$

This relation defines how $|W_\psi[F](x, s)|$ decays when the scale s goes to zero. From the WT, we can therefore recover the local Hölder exponent of the function F.

The multi-scale wavelet analysis to extract the holder exponent h

We use here modified versions of the definition (Eq. (7)) of the WT that gives directly a measure of F in nN, dF/dZ in nN/nm and d^2F/dZ^2 in Pascal smoothed by a Gaussian window of width s:

$$\mathcal{T}_{g^{(0)}}[F](b,s) = W_{g^{(0)}}[F](b,s) \quad (11)$$

$$\mathcal{T}_{g^{(1)}}[F](b,s) = \frac{1}{s} W_{g^{(1)}}[F](b,s) \quad (12)$$

$$\mathcal{T}_{g^{(2)}}[F](b,s) = \frac{1}{s^2} W_{g^{(2)}}[F](b,s)\ . \quad (13)$$

Then the local power-law extracted from the WT (Eq. 10) for the first order and second order derivatives is shifted by -1 or -2 depending of the formula that we choose to compute the transformation $\mathcal{T}_{g^{(i)}}[F](b,s)$, with $i = 1, 2$:

$$\mathcal{T}_{g^{(i)}}[F](x_0,s) \propto A s^{h-i}\ . \quad (14)$$

Wavelet multi scale analysis of the $h = 1$ piece wise linear model with $H_w = 0$ (Regime B alone)

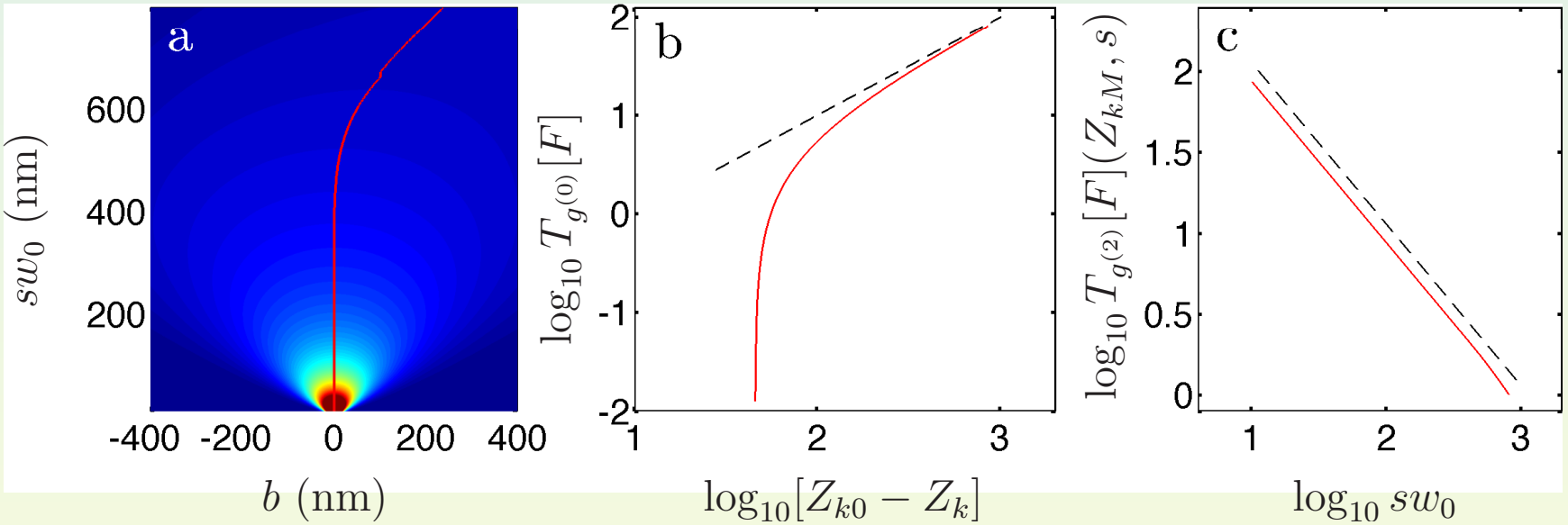

Computation of the first and second derivatives of a piece wise linear function using the WT method with a Gaussian function ($sw_0 = 10$ nm). (a) The original force curve. (b) $\mathcal{T}_{g^{(0)}}[F](Z_k - Z_{k0}, s = 1)$, Z_{k0} corresponds to $T_{contact} = -10^{-4}$ nN/nm (see text). (c) $\mathcal{T}_{g^{(1)}}[F](Z_k - Z_{k0}, s = 1)$ in nN/nm. (d) $\mathcal{T}_{g^{(2)}}[F](Z_k - Z_{k0}, s = 1)$ in MPa.

Wavelet multi scale analysis of the complete mathematical model

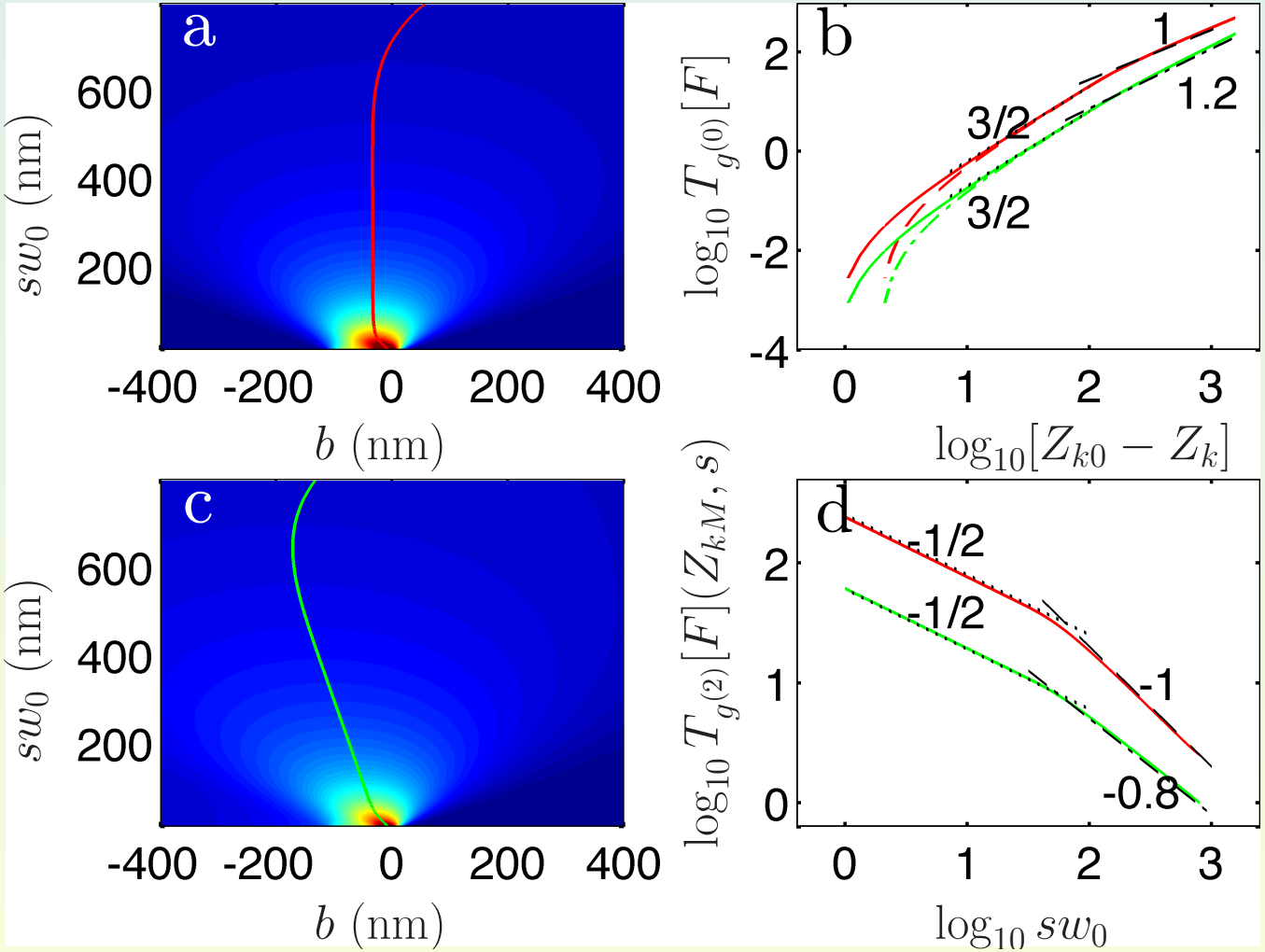

Wavelet based analysis of two theoretical forces curves. (a) and (c) Color coded representation (from 0: dark blue to 2MPa: red) of $\mathcal{T}_{g^{(2)}}[F](Z_k - Z_{k0}, s)$ computed from two of the force curves, corresponding to the Hölder exponents $h = 1$ (a) and $h = 1.2$

Wavelet multi scale analysis of experimental force curves

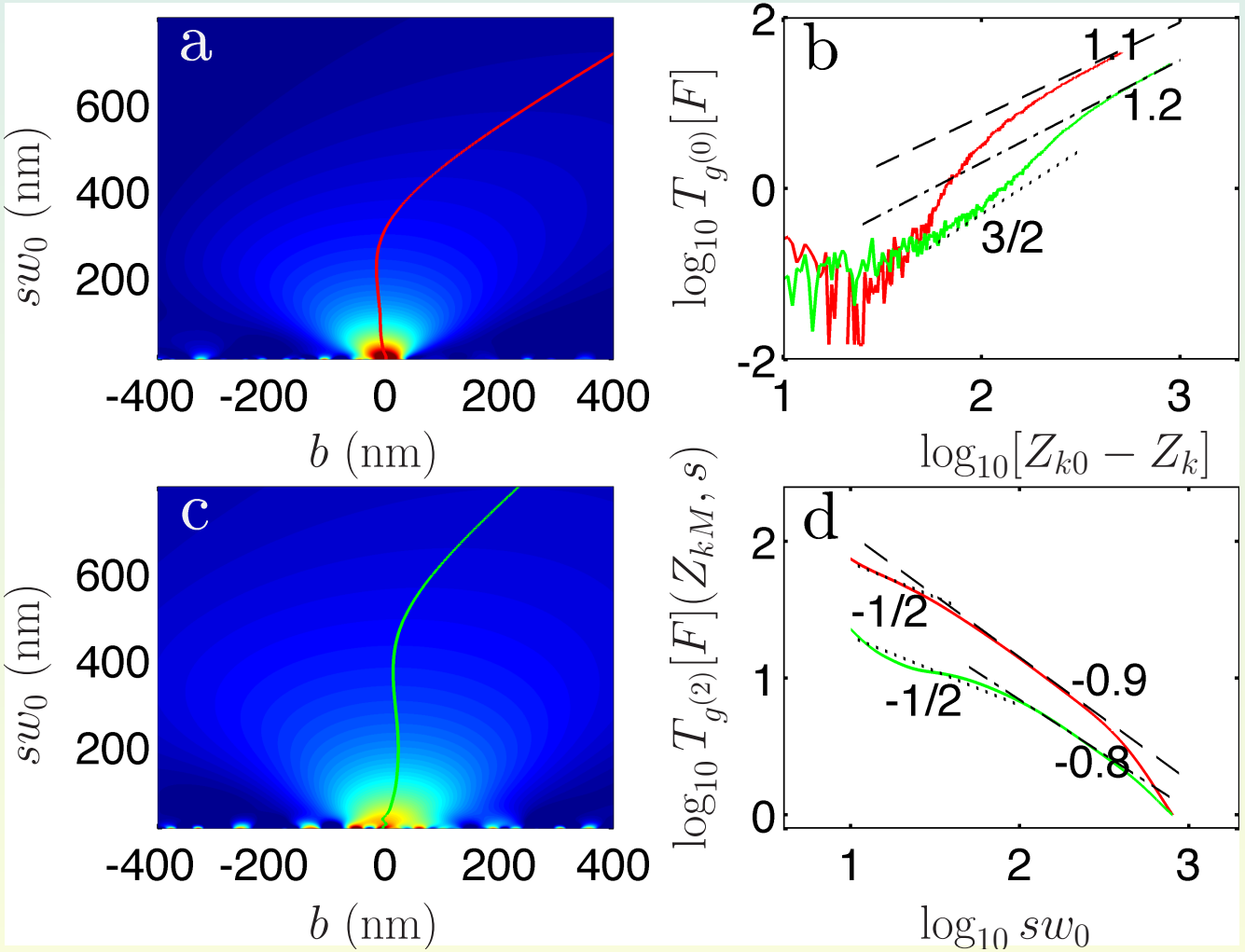

Wavelet based analysis of two experimental forces curves. (a) and (c) Color coded representation (from 0: dark blue to red: 500 kPa (a) and 150 kPa (b)) of $\mathcal{T}_{g^{(2)}}[F](b, s)$ computed from two force curves with the same color and line coding.

Statistics of mechanical parameters and scaling exponents: the turgescent cells

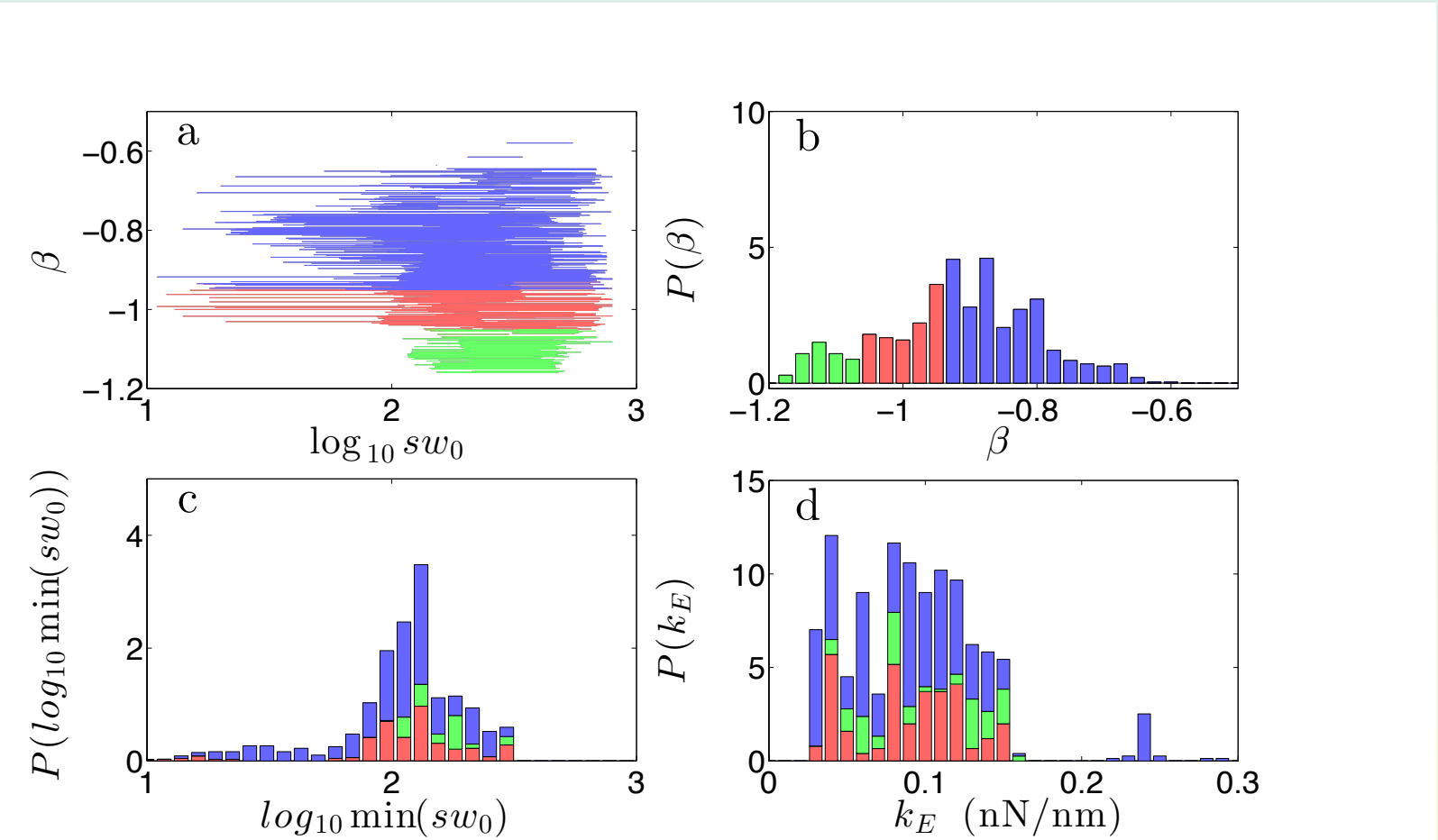

Statistical analysis of the mechanical properties of turgescent *A-thaliana* cell walls. (a) β exponents plotted versus the interval of scales sw_0 (in log scale). (b) Histogram of β values. Three intervals of β have been distinguished with different color codings. (c) Stacked histograms of the minimum scale sw_0 in $\log_{10}$ where the scaling exponent β was detected with a 1% accuracy. (d) Stacked histograms of effective stiffness k_E coefficient.

Fluorescence imaging of turgescent cells

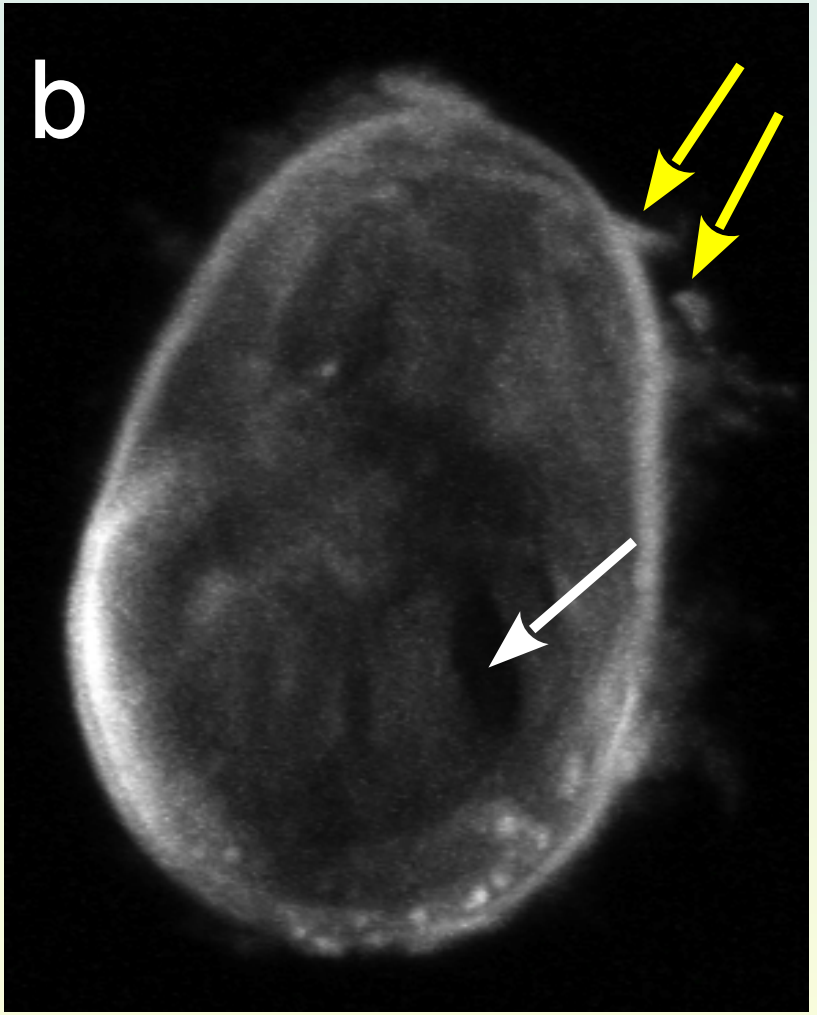

Confocal images of turgescent single *A. thaliana* cells. (a) Middle section of a cell expressing GFP-MBD (green) that marks microtubules and stained with Pontamine Fast Scarlet 4B (red) that marks cellulose. (b) 3D reconstruction of a half cell stained with Pontamine Fast Scarlet 4B (grey). The white arrow indicates a region with less cellulose and the yellow arrows indicate irregularities of the cell wall.

Statistics of mechanical parameters and scaling exponents: the plasmolyzed cells

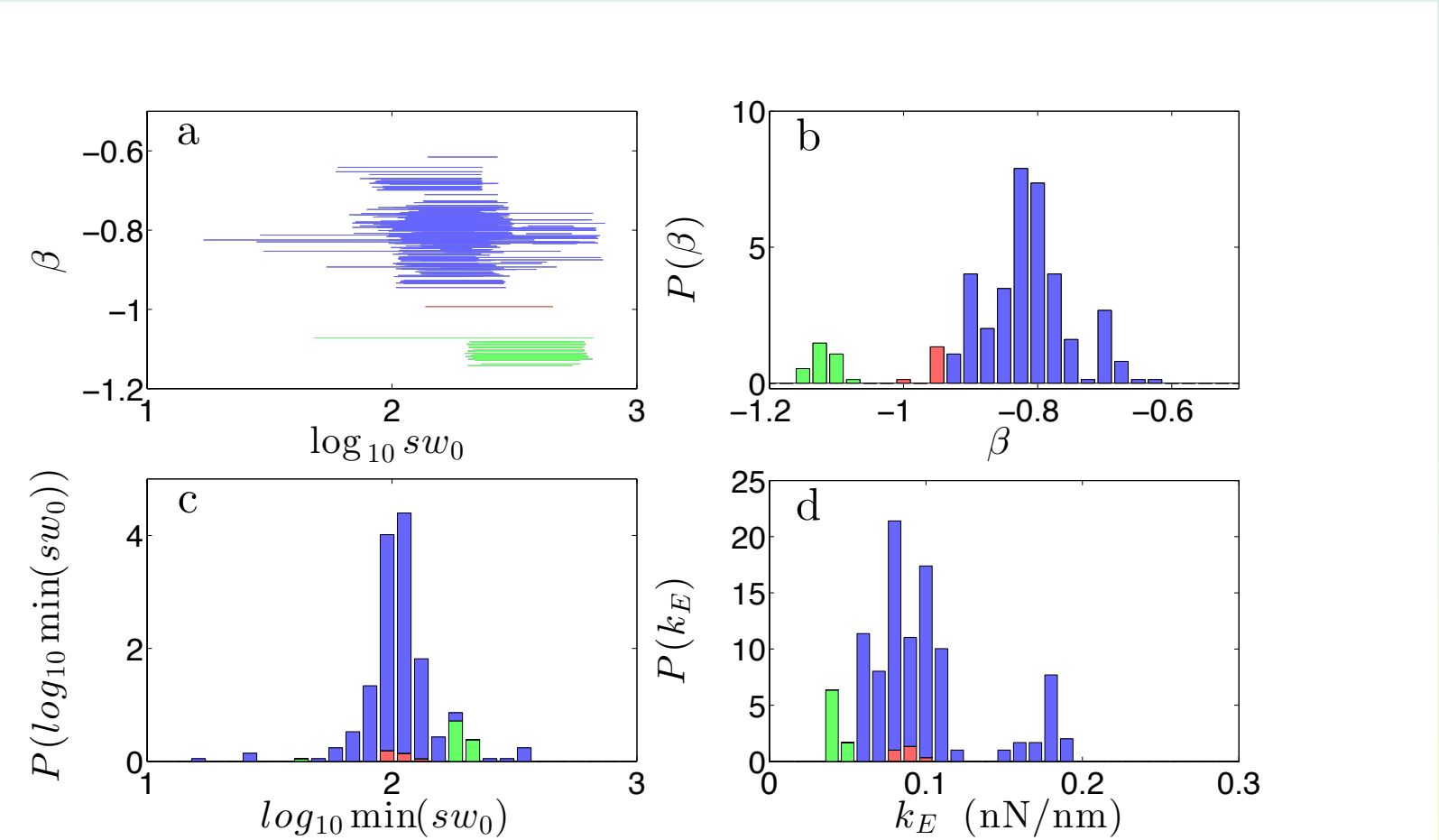

Statistical analysis of the mechanical properties of plasmolyzed *A-thaliana* cell walls (adding mannitol). (a) β exponents plotted versus the interval of scales sw_0 (in log scale). (b) Histogram of β values. Three intervals of β have been distinguished with different color codings. (c) Stacked histograms of the minimum scale sw_0 in $\log_{10}$ where the scaling exponent β was detected with a 1% accuracy. (d) Stacked histograms of effective stiffness k_E coefficient.

Statistics of mechanical parameters and scaling exponents: the cytolyses cells

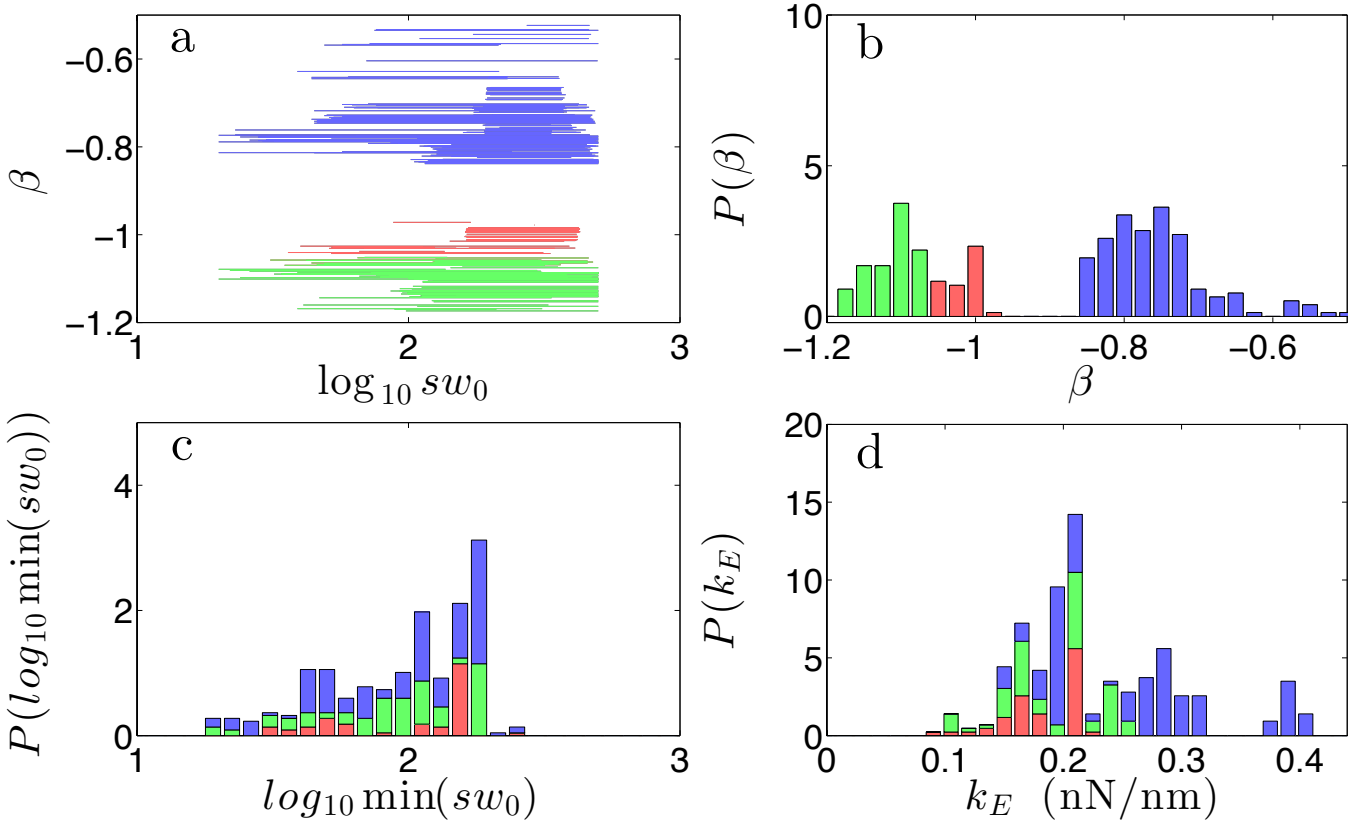

Statistical analysis of the mechanical properties of cytolyses *A-thaliana* cell walls (dilution with water of the culture medium). (a) β exponents plotted versus the interval of scales sw_0 (in log scale). (b) Histogram of β values. Three intervals of β have been distinguished with different color codings. (c) Stacked histograms of the minimum scale sw_0 in $\log_{10}$ where the scaling exponent β was detected with a 1% accuracy. (d) Stacked histograms of effective stiffness k_E coefficient.

Fluorescence imaging of plasmolyzed and cytolyses cells

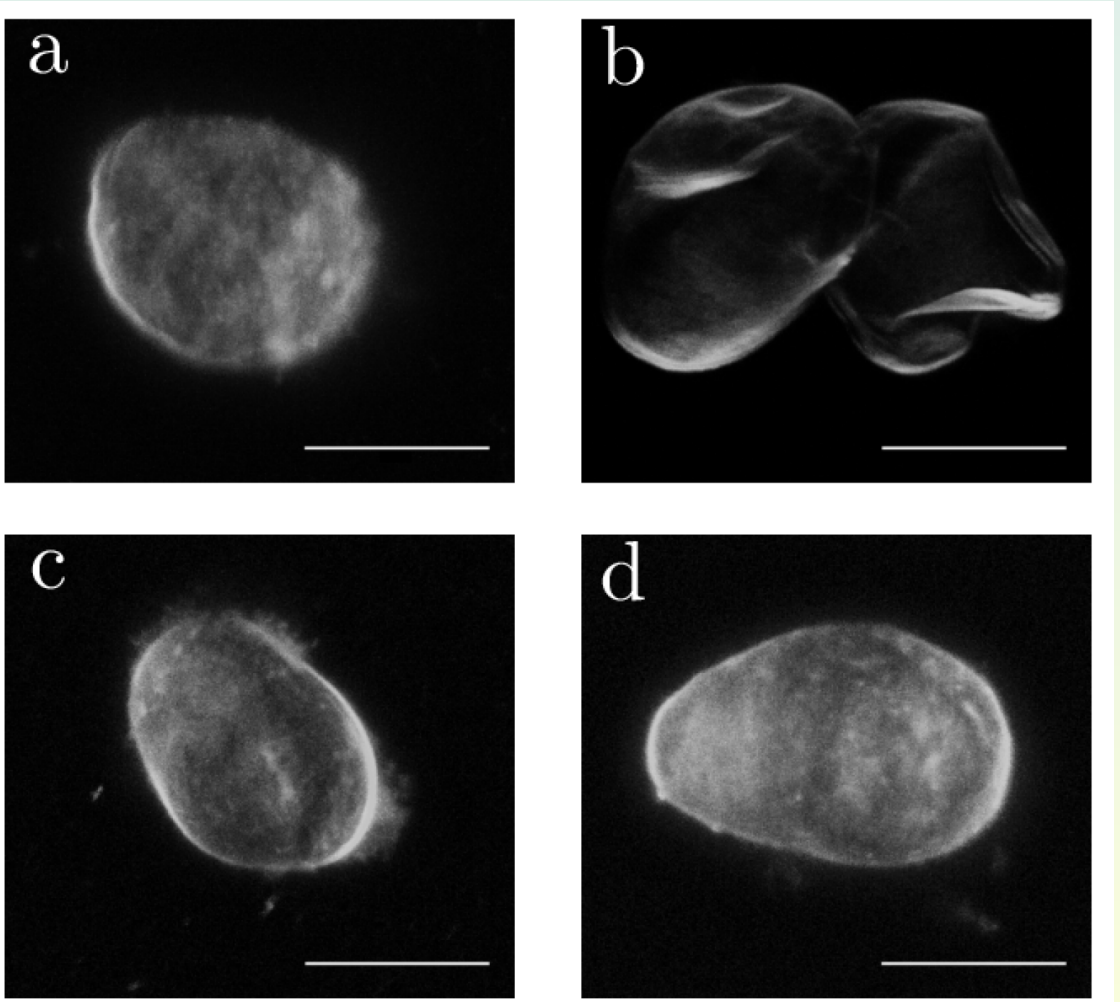

Confocal images of plasmolyzed and cytolysed single *A. thaliana* cells. (a) and (b): two examples of plasmolyzed cells. (c) and (d): two examples of cytolyses cells. 3D reconstruction of a half cell stained with Pontamine Fast Scarlet 4B (grey).

Reconstructing a map of mechanical exponents on a single turgescent cells

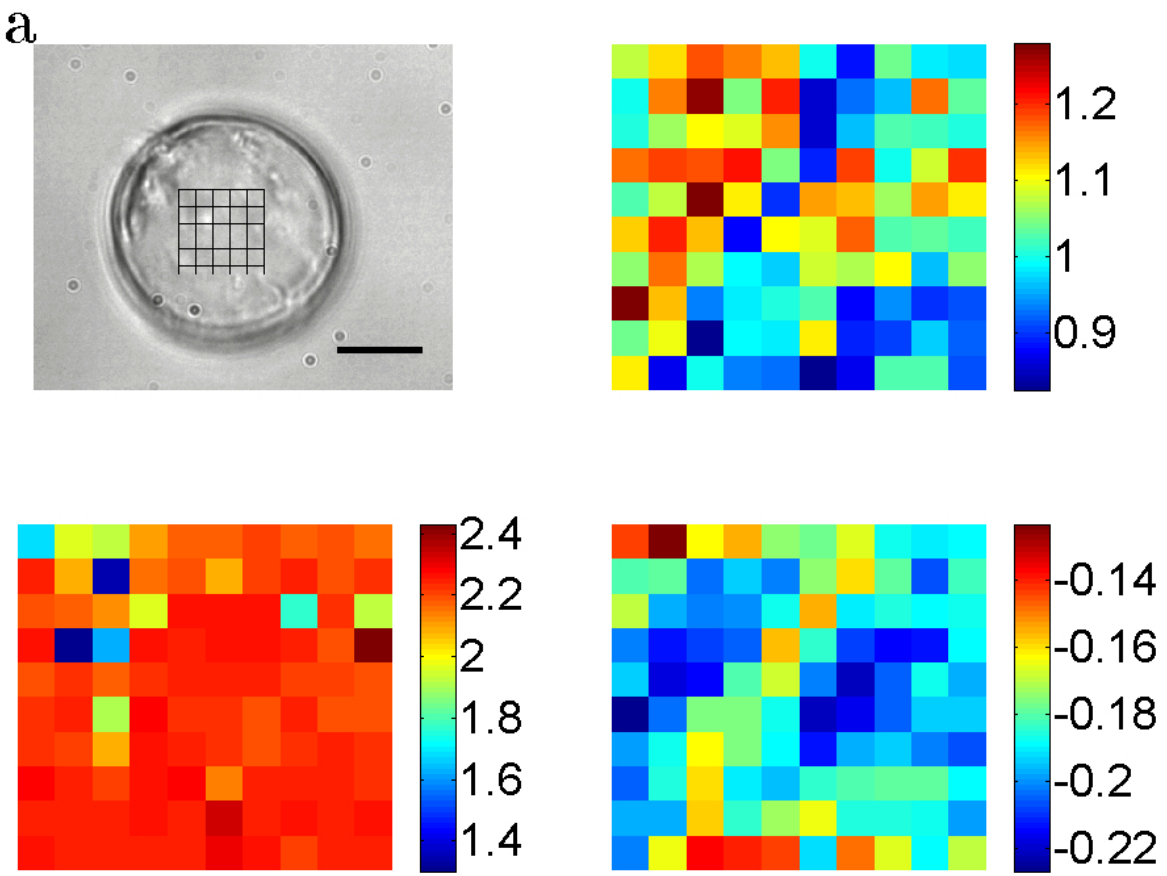

The corresponding statistical study from the single turgescent cell

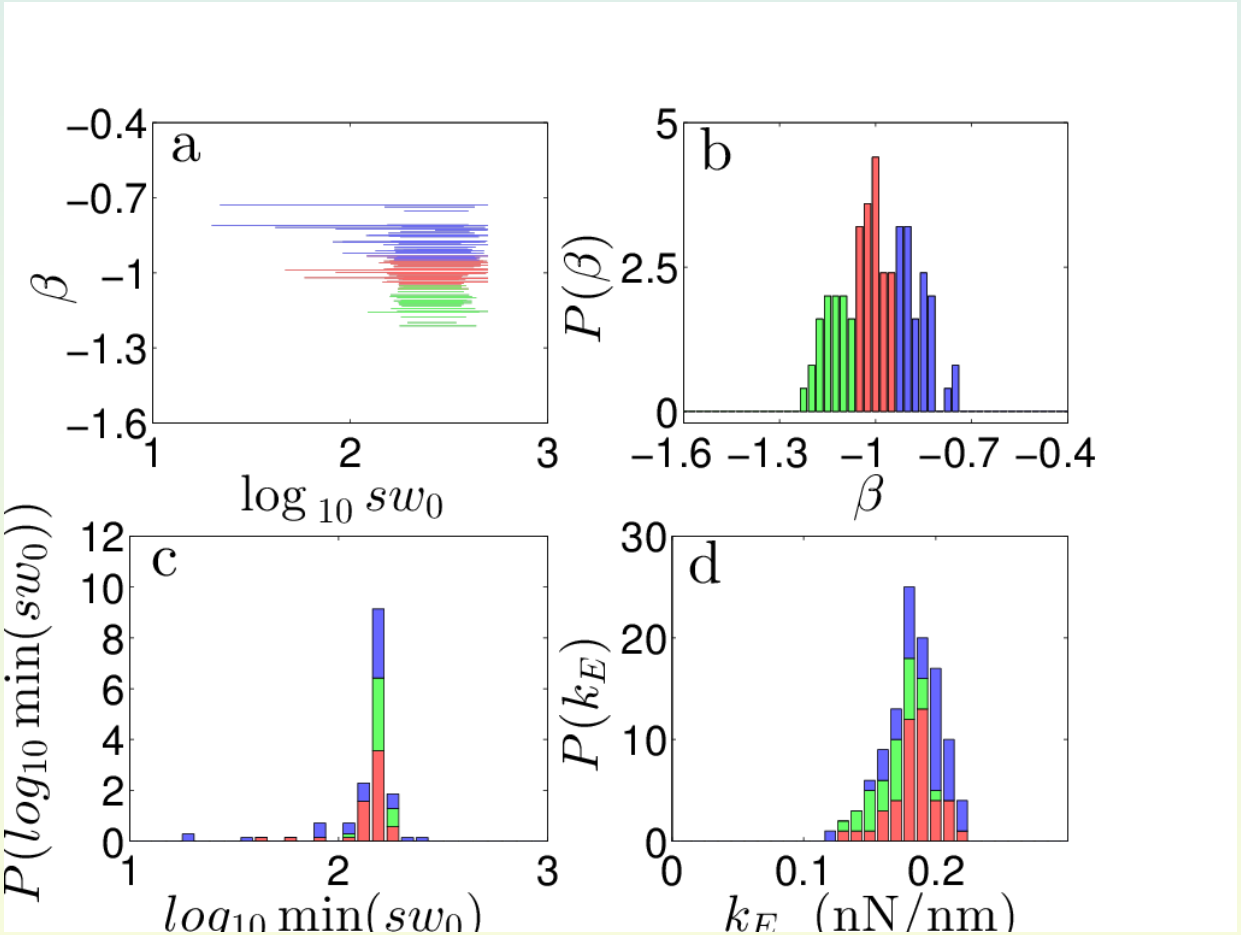

Statistical analysis of the mechanical properties of a single turgescent *A-thaliana* cell wall. (a) β exponents plotted versus the interval of scales sw_0 (in log scale). (b) Histogram of β values. Three intervals of β have been distinguished with different color codings. (c) Stacked histograms of the minimum scale sw_0 in $\log_{10}$ where the scaling exponent β was detected with a 1% accuracy. (d) Stacked histograms of effective stiffness k_E coefficient.